Early Galaxy Formation and Evolution Through the Eyes of New Facilities

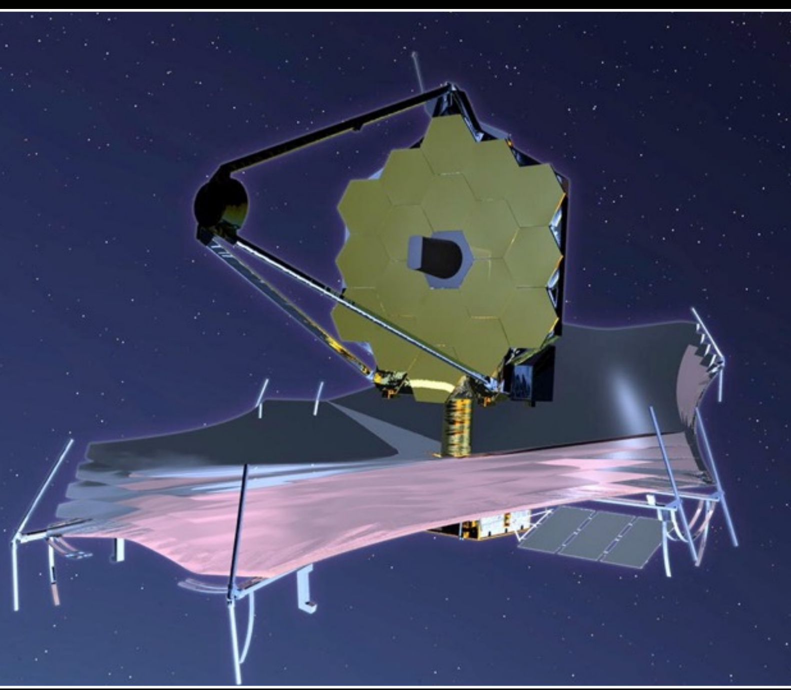

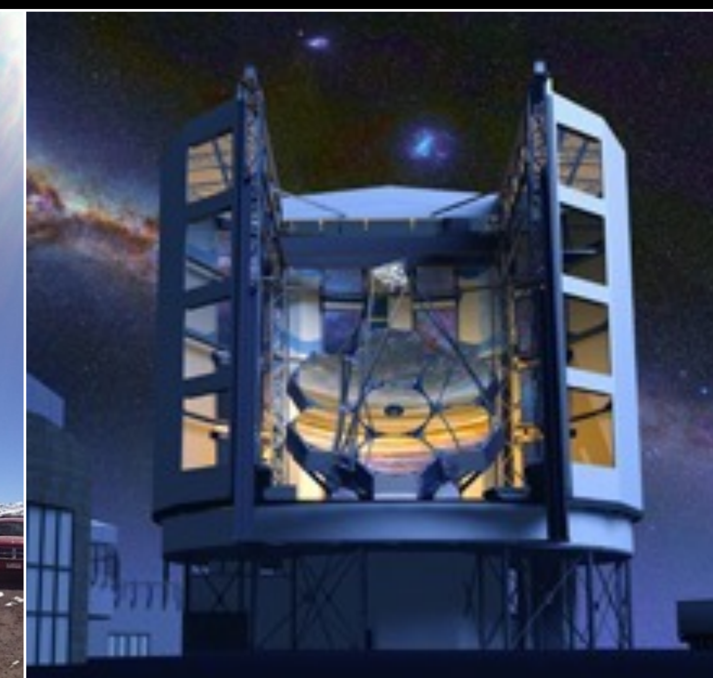

Brant Robertson
University of Arizona

Brief History of the Universe

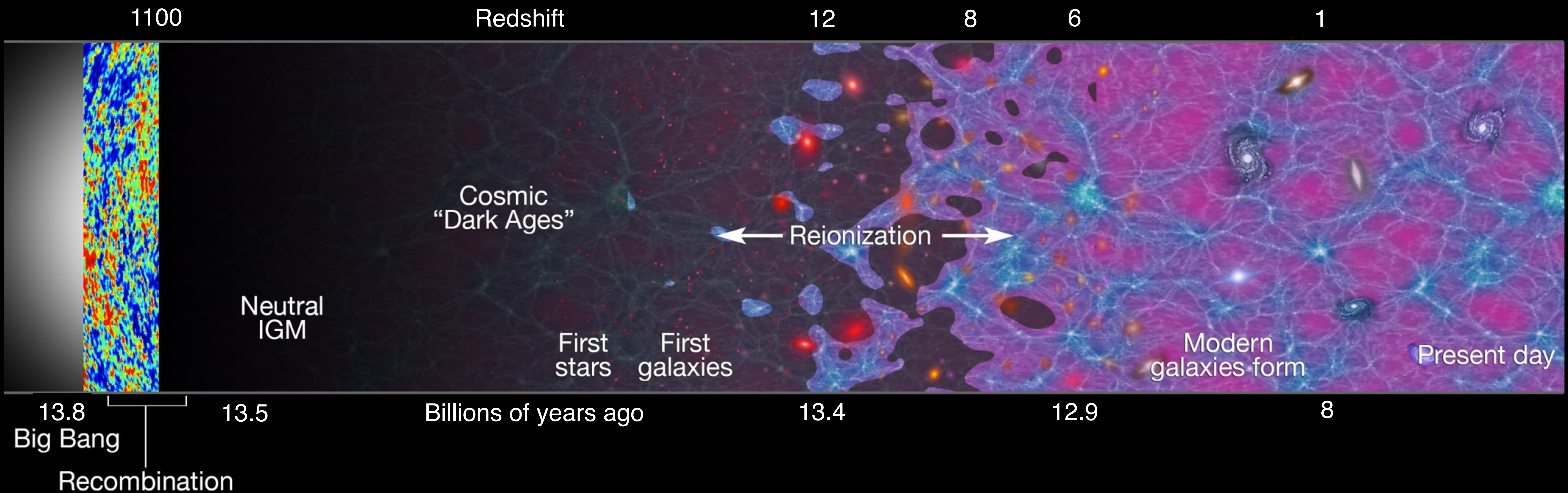

Adapted from Robertson et al. *Nature*, **468,** 49 (2010).

Observational Facilities Over the Next Decade

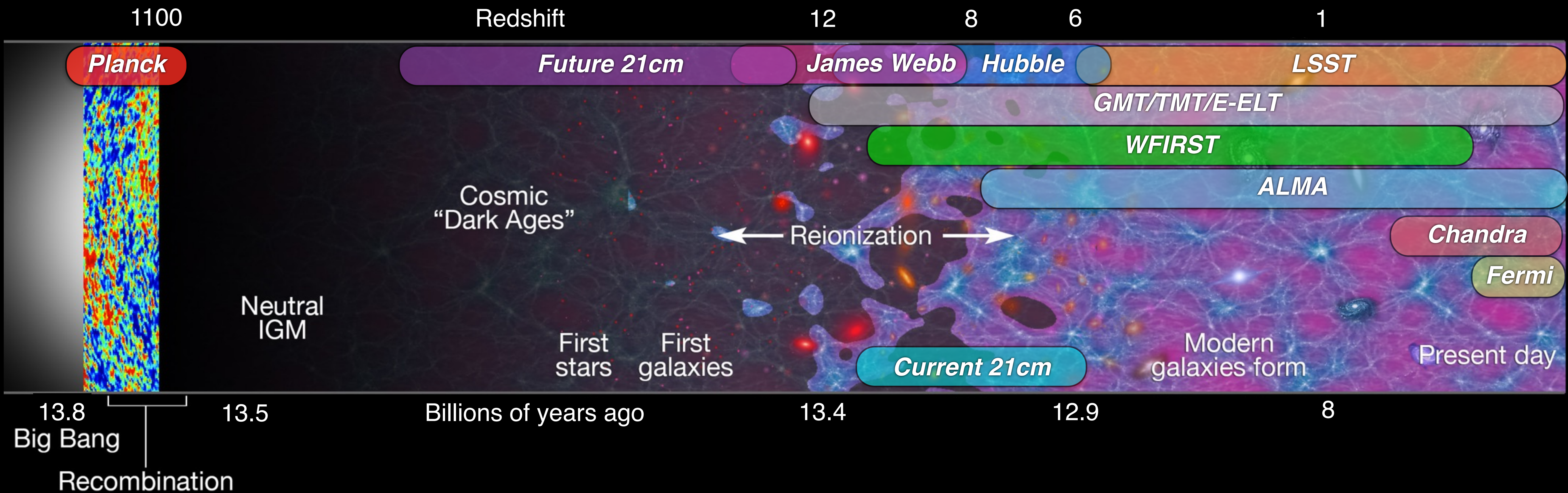

Observations with ALMA, JWST, LSST, GMT/TMT/E-ELT, and WFIRST will drive astronomical discoveries over the next decade.

Adapted from Robertson et al. *Nature*, **468,** 49 (2010).

JWST

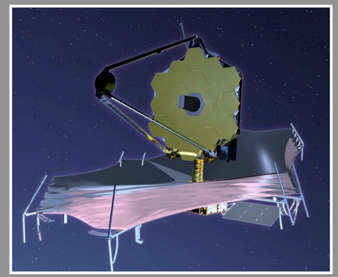

hi res, NIR, spectroscopy space-based

- 6.4m mirror in 18 segments
- 0.6-5μm NIRCam (30AB)
- 5-28.5μm MIRI
- R~100, 1000, 2700 @ 1-5μm

LSST

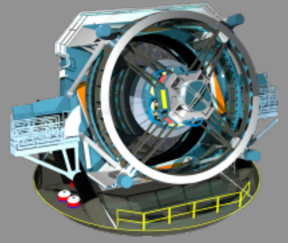

wide area, optical, ground-based

- 8.4m with embedded tertiary
- 3.2 Gpixel camera; 60PB raw
- 18,000 deg^2 *ugrizy AB=26.7*
- 4x 9.6 deg^2 *ugrizy* AB>28

ALMA

hi res, (sub)mm, spectroscopy ground-based

- 66 x 12m antennae
- 0.3-9.6mm observations
- 15-18km baselines
- up to 0.005 arcsec resolution

WFIRST

wide area, NIR, R~600, space-based

- 2.4m AFTA design from SDO
- 0.28 deg^2 *ZYJHF* detector
- 2,000 deg^2 *YJHF* AB=26.7
- 5-27.44 deg^2 2b AB=27-29

TMT

hi res, NIR, spectroscopy, ground-based

- 30m segmented primary
- 15 arcmin FOV, 0.3-28μm
- NIR diffraction limited
- AO fed spectroscopy

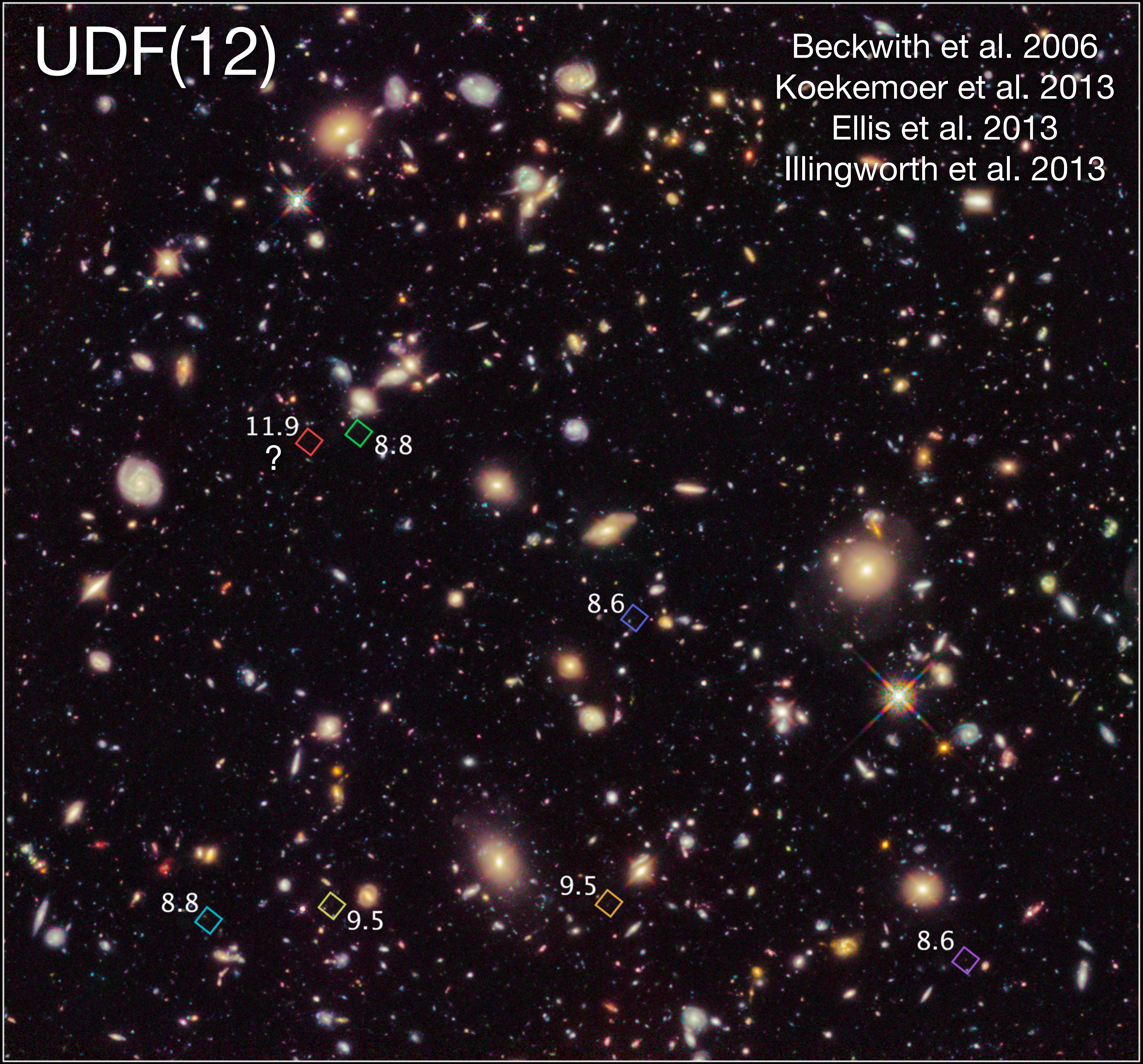

UDF(12)
Beckwith et al. 2006
Koekemoer et al. 2013
Ellis et al. 2013
Illingworth et al. 2013
11.9
?
8.8
8.6
8.8
9.5
9.5
8.6

Multi-Cycle Treasury Programs

CANDELS: Cosmic Assembly Near-infrared Deep Extragalactic Legacy Survey

Grogin et al., ApJS, 197, 35 (2011)
Koekemoer et al., ApJS, 197, 36 (2011)

CLASH: The Cluster Lensing and Supernova Survey with Hubble
Postman et al., ApJS, 199, 25 (2012)

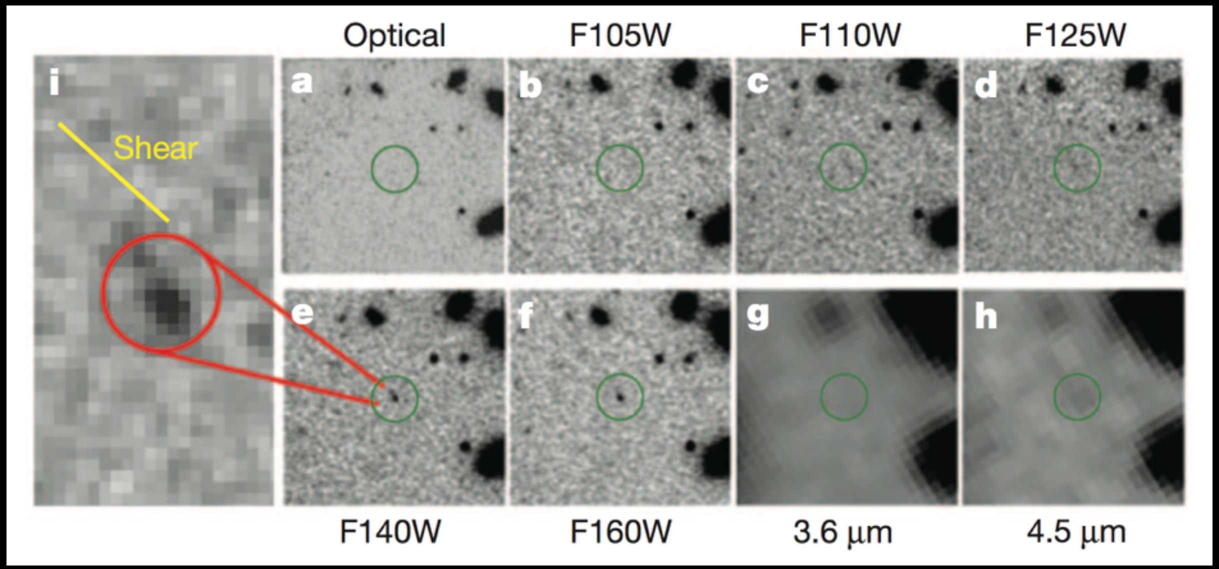

z~9 Candidate; Zheng et al., Nature, 489, 406 (2012)

FRONTIER FIELDS

- 6 Lensing clusters with ACS F435W, F606W, F814W and WFC3 F105W, F125W, F140W, and F160W (~28.8AB)

- Total of 840 orbits fully implemented

- Community funded to produce publicly-released gravitational lensing magnification maps.

- Observations compete for two clusters (Abell 2744, MACS J0416-2403)

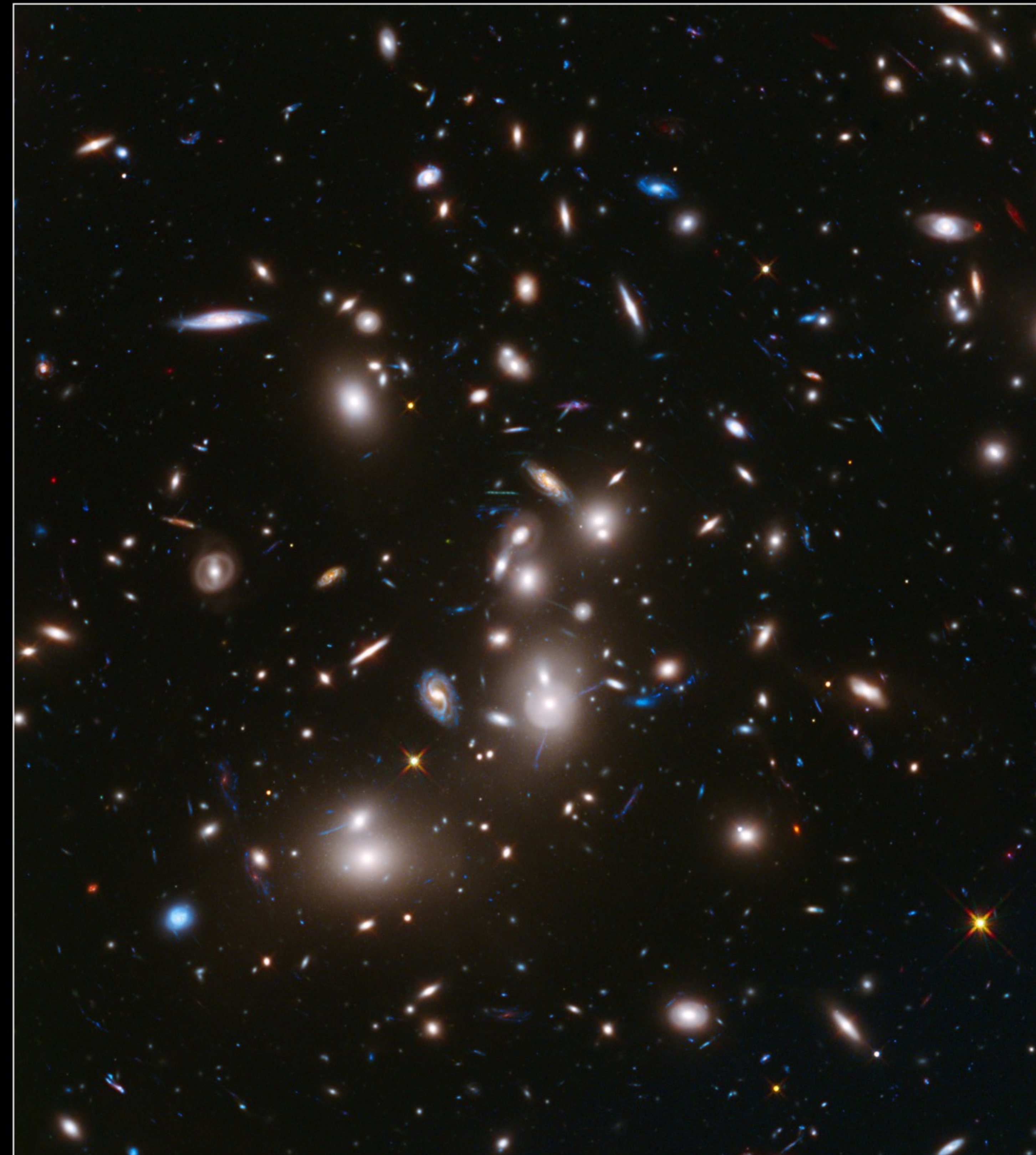

Hubble Frontier Field Abell 2744
Hubble Space Telescope • ACS • WFC3

NASA and ESA

STScI-PRC14-01a

Continuing the High-z Galaxy Search with the Frontier Fields

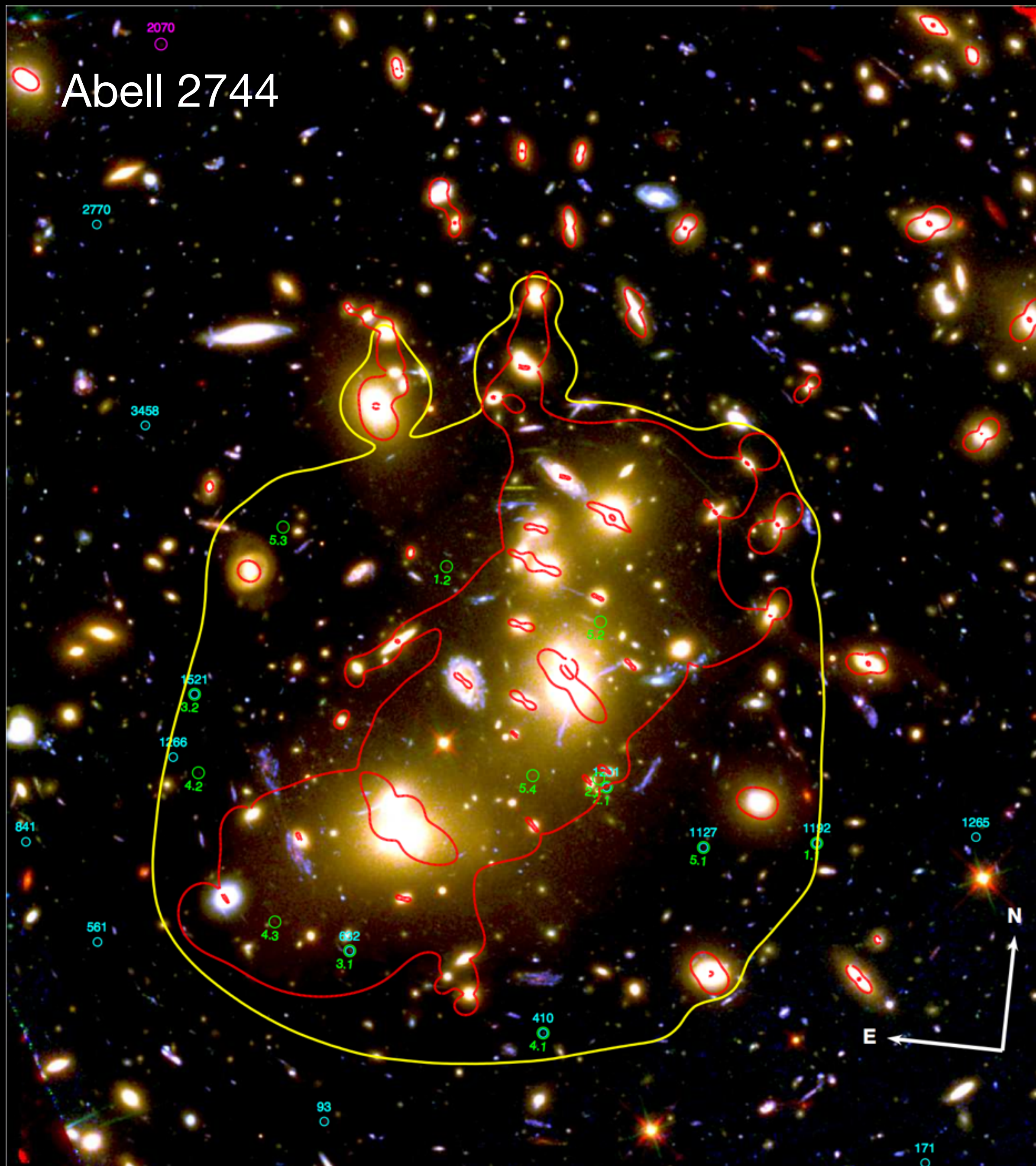

Atek et al. arXiv:1311.7670

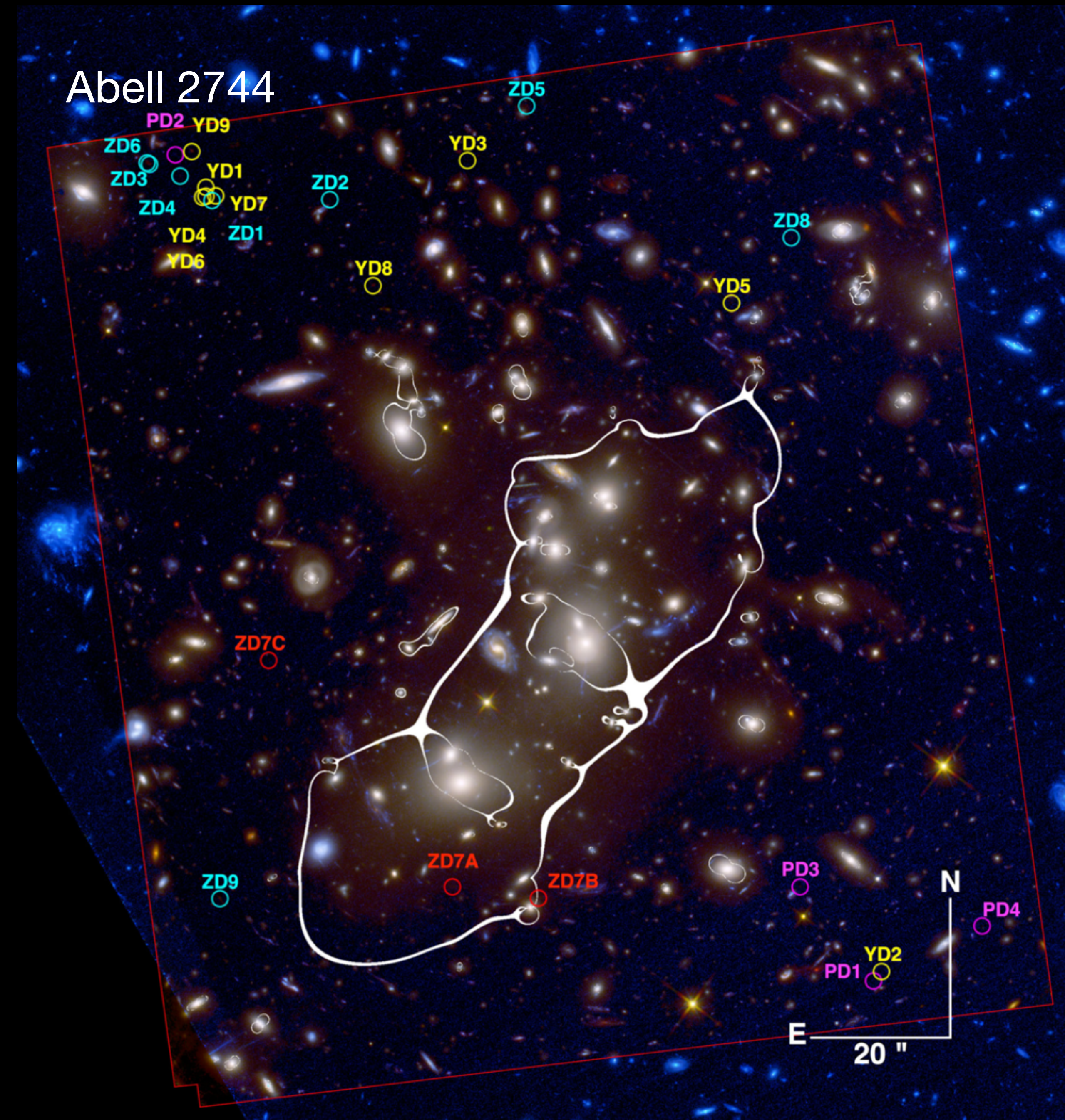

Zheng et al. arXiv:1402.6743

- DDT Hubble program to observe deeply gravitational lensing galaxy clusters.
- 70 ACS and 70 WFC3 orbits per cluster, sufficient for finding high-z galaxies.
- 16-18 z>6.5 galaxies claimed in Abell 2744, more to come.

UV Luminosity Function @ z~7

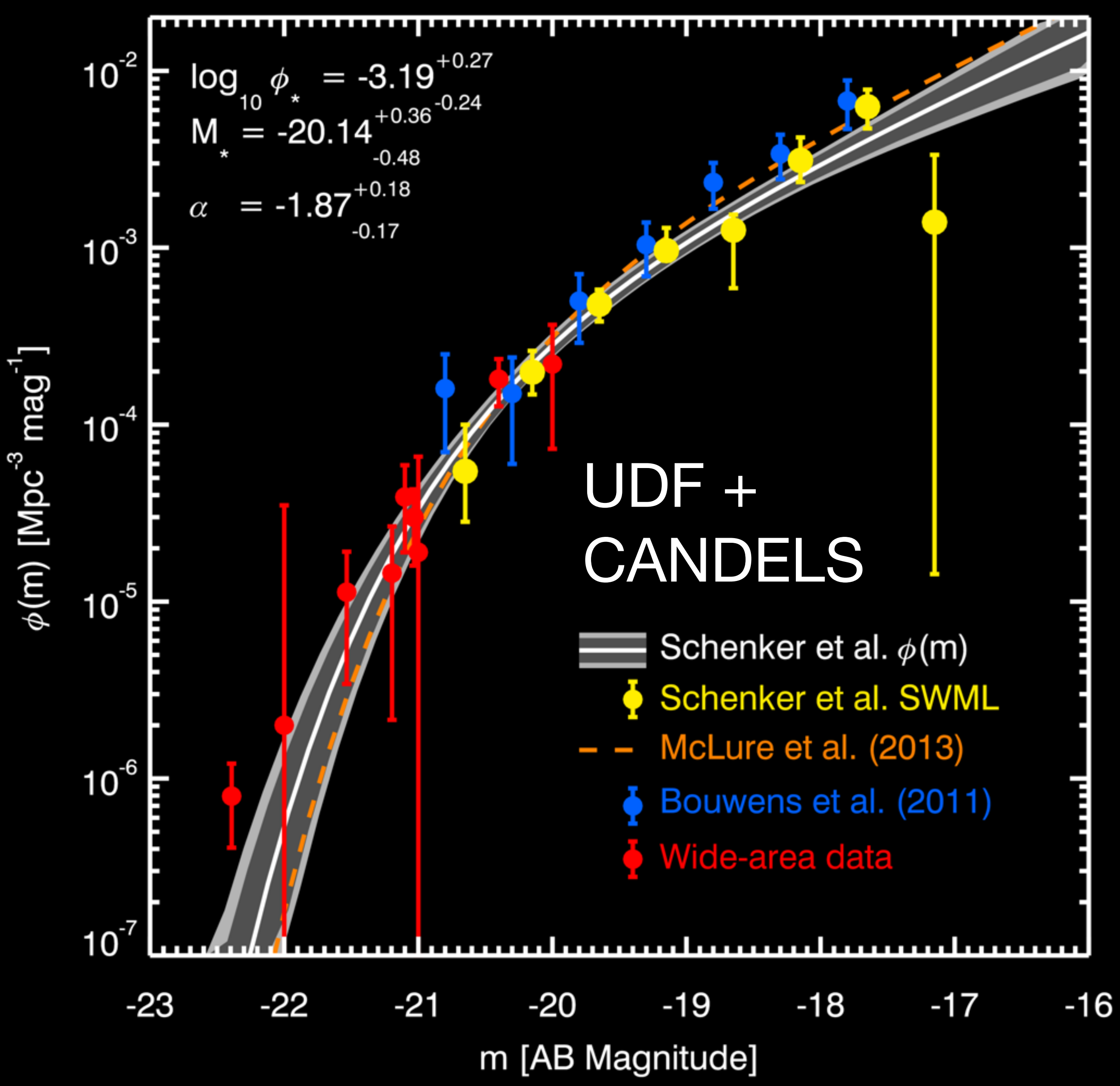

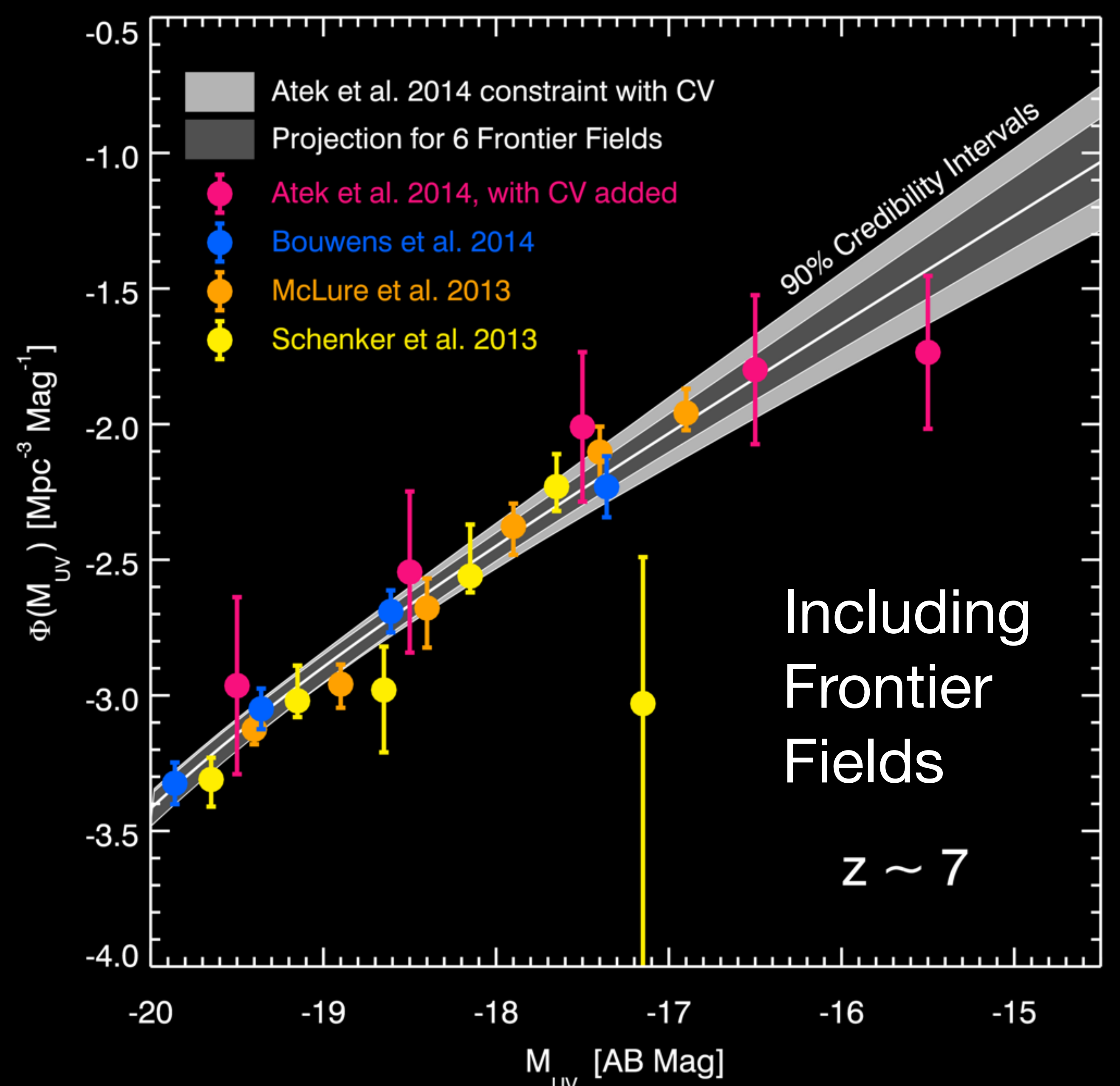

Schenker, BER, et al., ApJ, 768, 196 (2013)

BER, et al., ApJL, 796, 27 (2014)

Physical Ingredients of Reionization

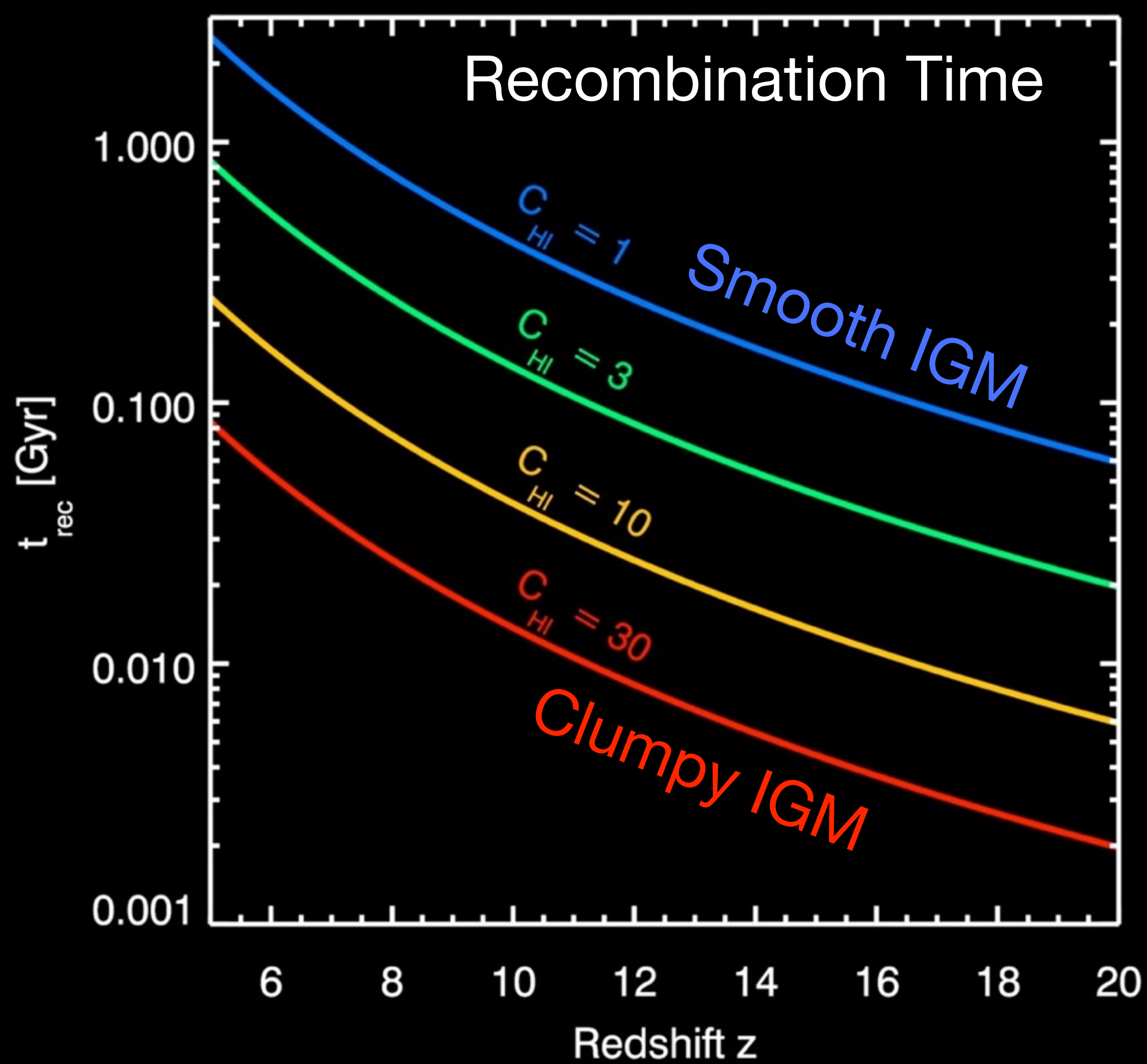

Ionization Fraction Evolution

Ionizing photon production rate (density)

$$\dot{Q}_{\rm HII} = \frac{\dot{n}_{\rm ion}}{\langle n_{\rm H} \rangle} - \frac{Q_{\rm HII}}{t_{\rm rec}}$$

Comoving H density

Recombination time

Ionizing Photon Density

$$\dot{n}_{\rm ion} = f_{\rm esc}\xi_{\rm ion}\rho_{\rm UV}$$

Escape fraction

Ionizing photons per UV luminosity

Comoving UV luminosity (SFR) density

Recombination Time

$$t_{\rm rec} = \left[C_{\rm HII}\alpha_{\rm B}(T)(1 + Y_{\rm p}/4X_{\rm p})\langle n_{\rm H}\rangle(1+z)^3\right]^{-1}$$

Clumping factor

Case B recombination coefficient

Helium fraction

Clumping Factor

$$C_{\rm HII} \equiv \frac{\langle n_{\rm HII}^2 \rangle}{\langle n_{\rm HII} \rangle^2}$$

~1-6 (Pawlik et al. 2009)

Madau et al. 1998, Bolton & Haehnelt 2007

Star Formation History of the Universe

Star formation history from UV (blue) and IR (red) observations, adopted from Madau & Dickinson (2014).

We can use this star formation history of the universe to compute the reionization history of the IGM.

BER, et al., ApJL, accepted
arXiv:1502.02024

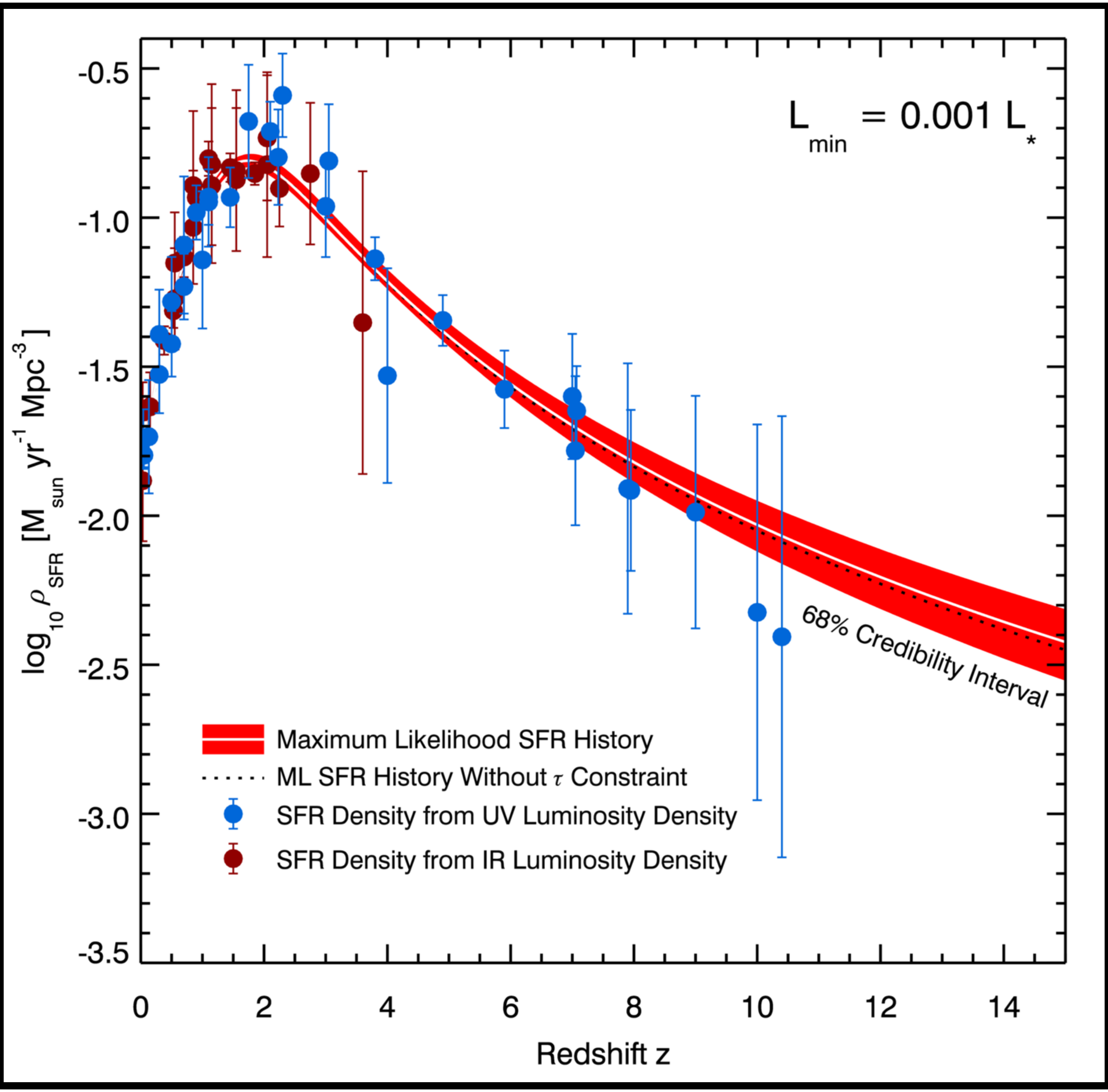

Reionization History Implied by High-z Star Formation

IGM Neutral Fraction, shown with constraints from a variety of independent probes**.**

Galaxies with L_{UV}>0.001L*
are sufficient to reionize the Universe by z~6 (red band). (red band), consistent with other IGM neutrality probes.

Forced match to WMAP Thomson optical depth constraints (orange) requires earlier reionization with same assumptions, not consistent with IGM neutrality constraints.

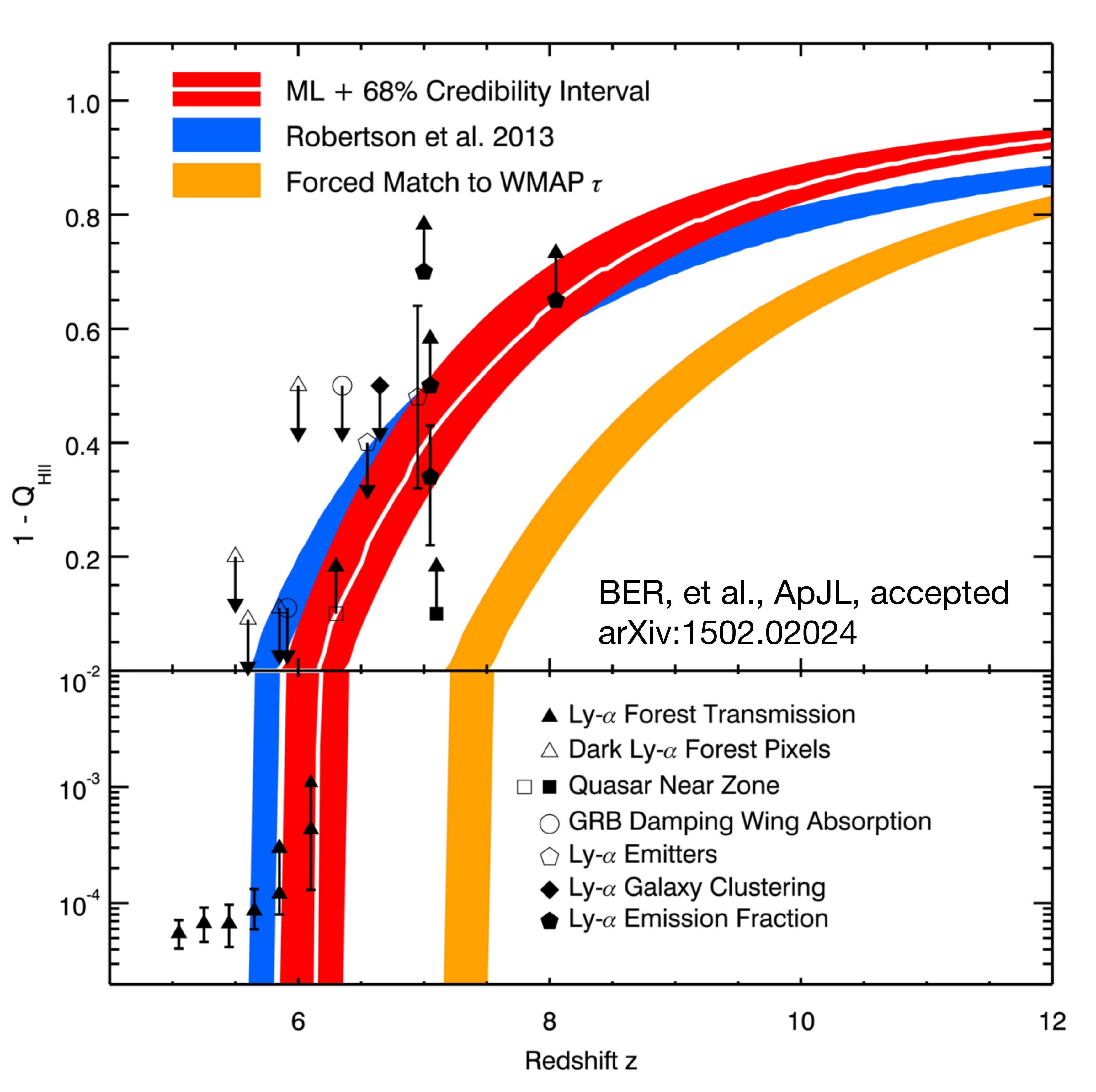

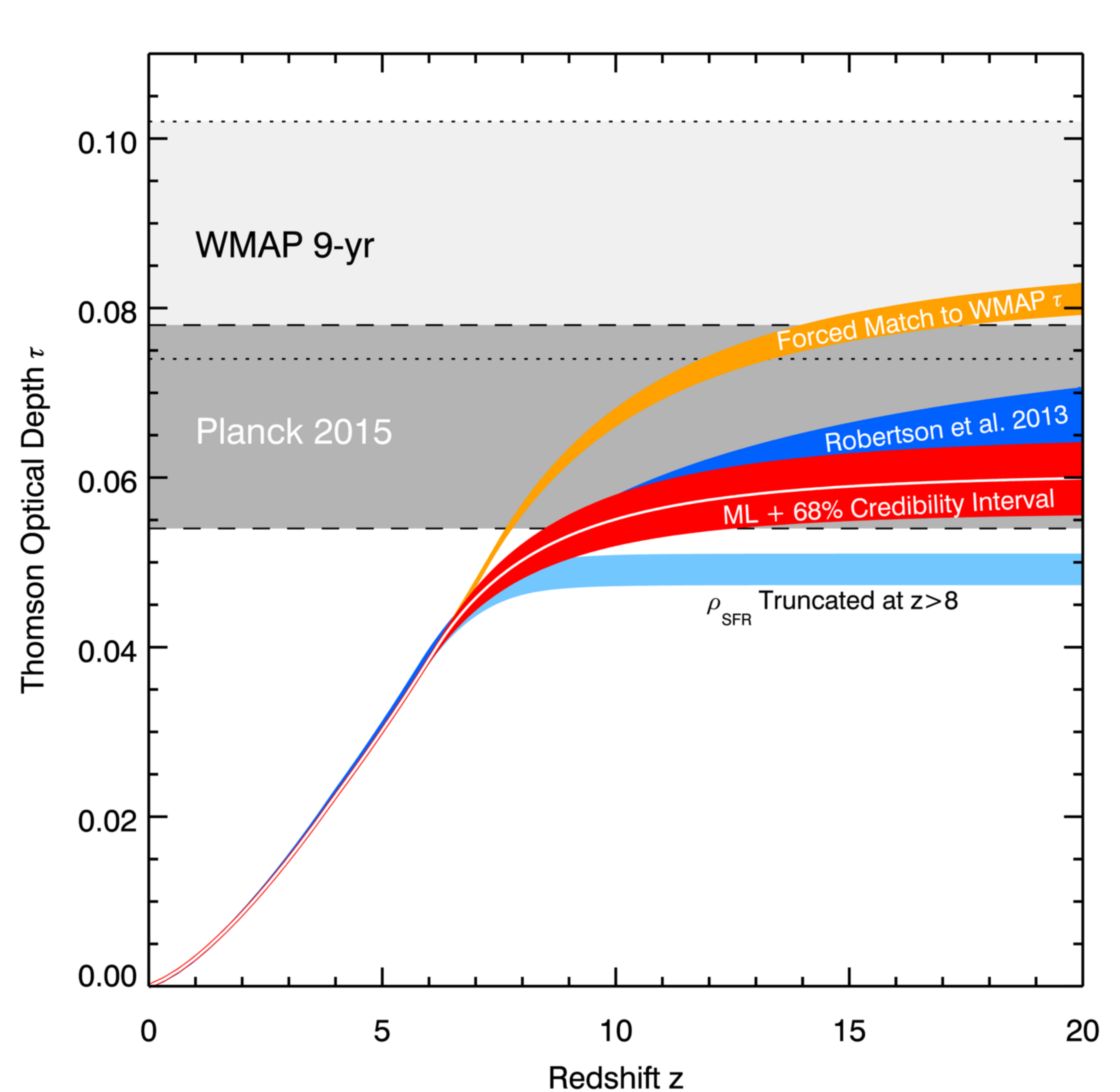

Thomson Optical Depth to Electron Scattering

Recent Planck results suggest the Thomson optical depth to the CMB is tau ~ 0.065, substantially less than found by WMAP.

The Thomson optical depth provided by the high-z IGM ionized by star forming galaxies is now fully consistent with the CMB constraints (Robertson et al. 2015).

BER, et al., ApJL, accepted
arXiv:1502.02024

Implications for High-Redshift Galaxy Observations with James Webb Space Telescope

The Thomson scattering signal in the CMB suggests the presence of high-redshift galaxies.

We expect ~0.4-0.5 z>10 galaxies per square arcminute, detectable with JWST in the first deep exposures — ***we should find 5-10 z>10 galaxies in the first year of JWST operations.***

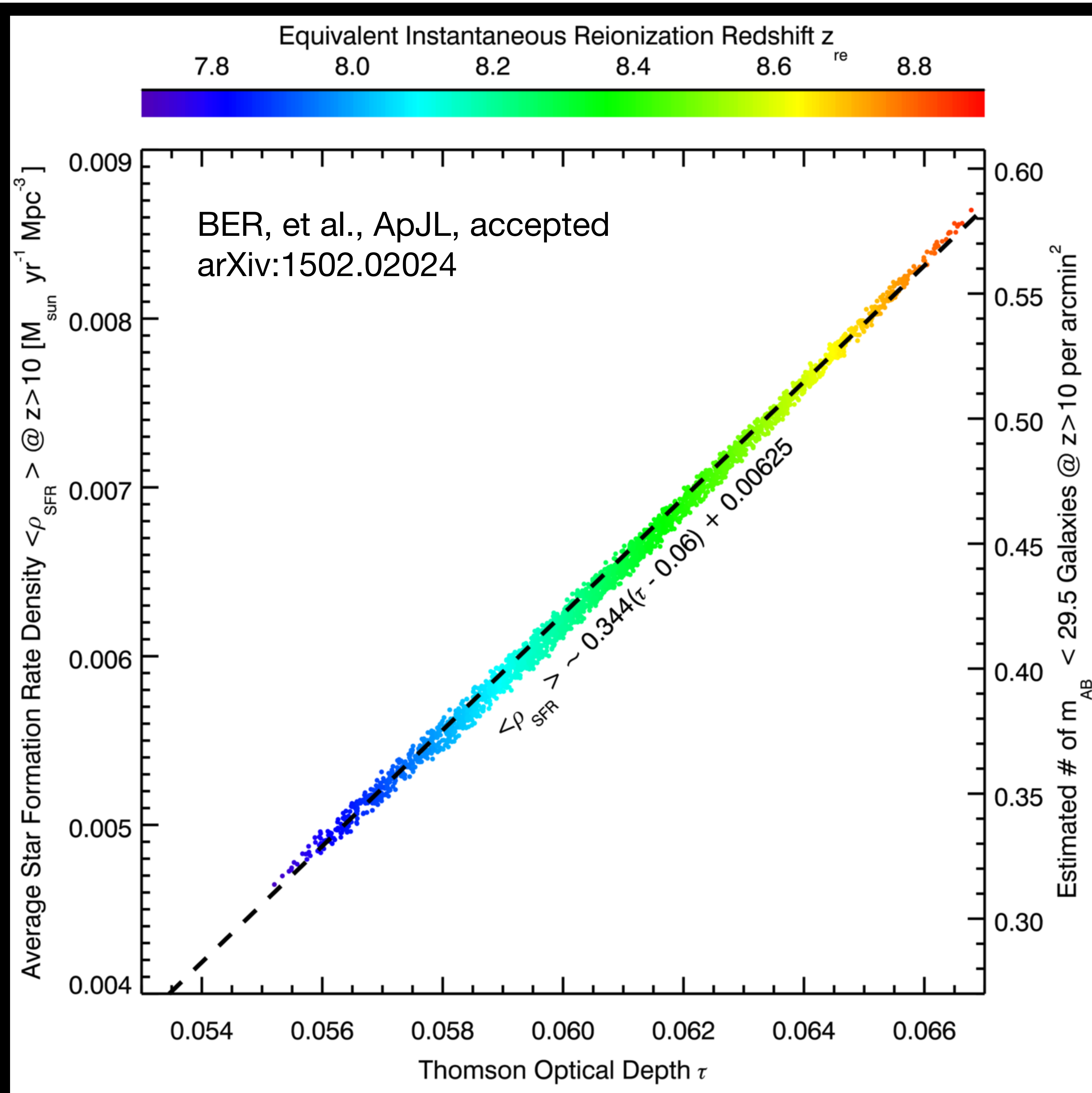

Observations of Distant Galaxies with James Webb Space Telescope

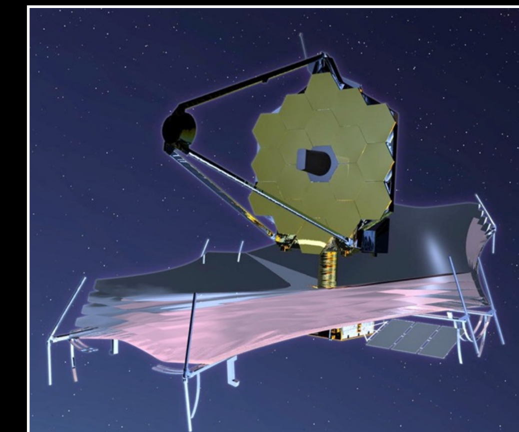

The amazing array of capable instruments on JWST will enable truly synergistic surveys of the high-redshift universe!

NIRCam

NIRISS

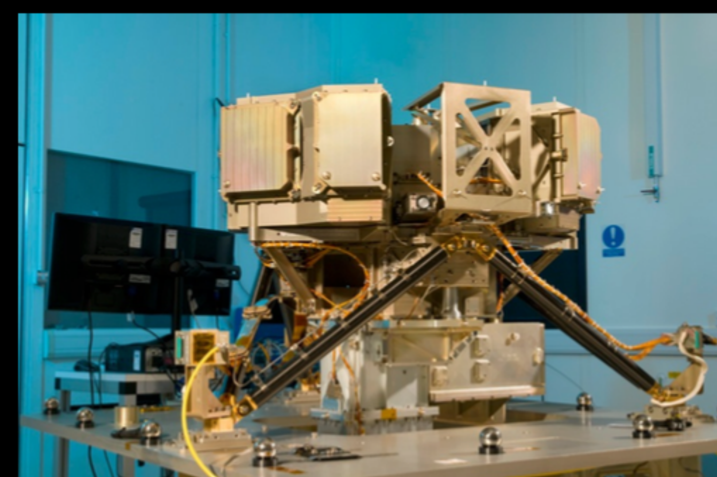

MIRI

NIRSpec

- Spectroscopic confirmation of high-redshift galaxies with NIRSpec, MIRI, NIRISS, NIRCAM
- Spectral signatures of star formation rates and metallicity for high-redshift galaxies
- Clustering of high-redshift galaxies
- Multi-tier depth/area designs for distant galaxy surveys

JWST NIRCam

- Simultaneous imaging in “red” (LW) and “blue” (SW) filters in two detector modules.
- Sensitivity is ~29AB in 10^4s @ 2μm
- Pixel scale in SW and LW arms give Nyquist sampling of PSF @ 2μm & 4μm

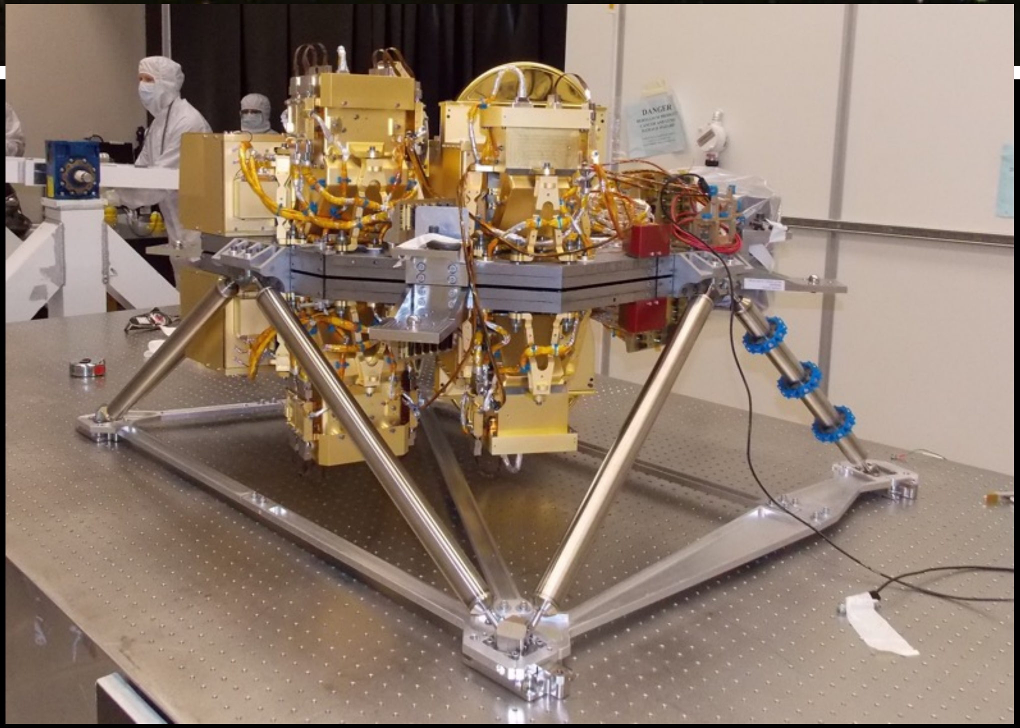

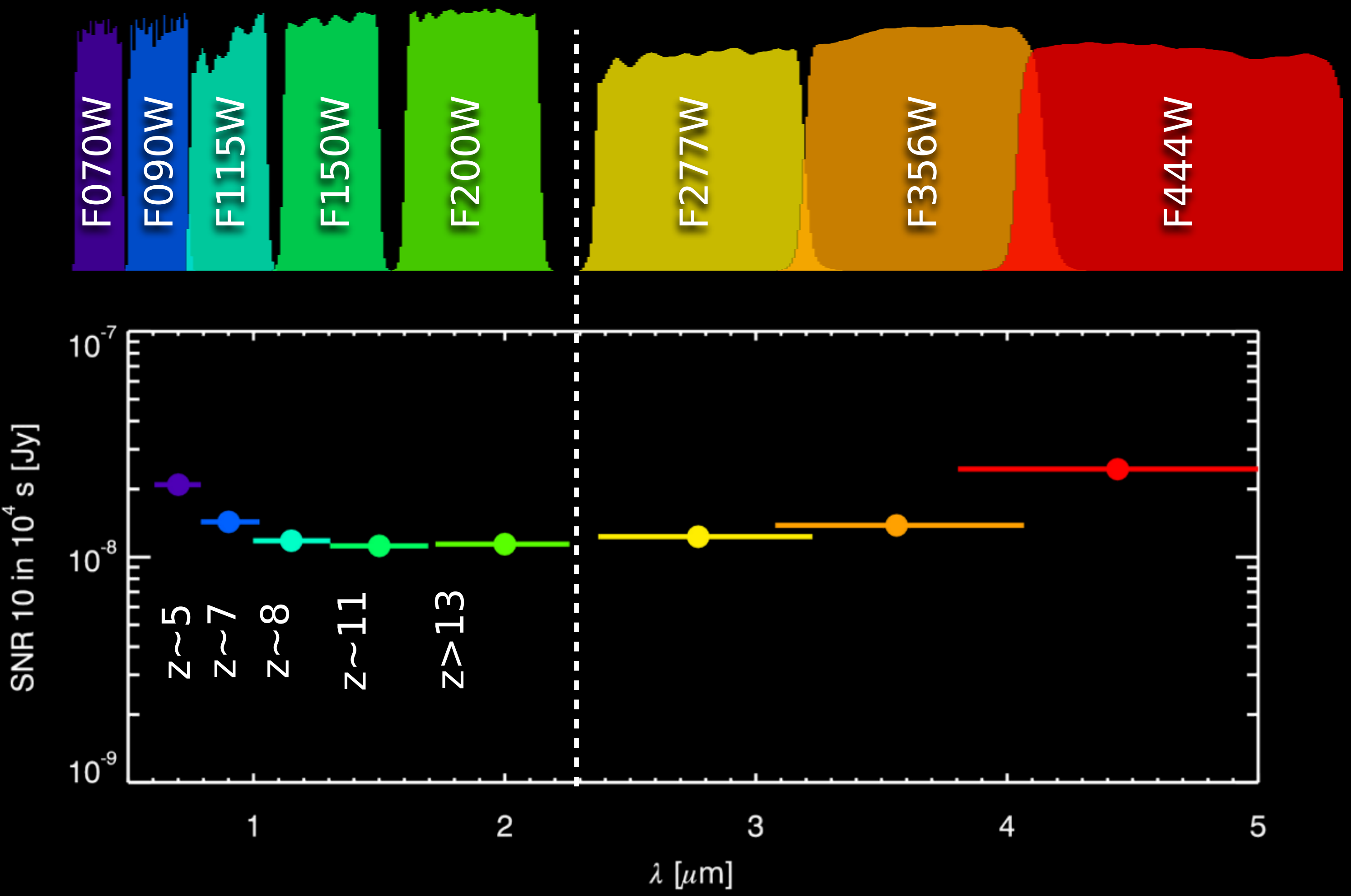

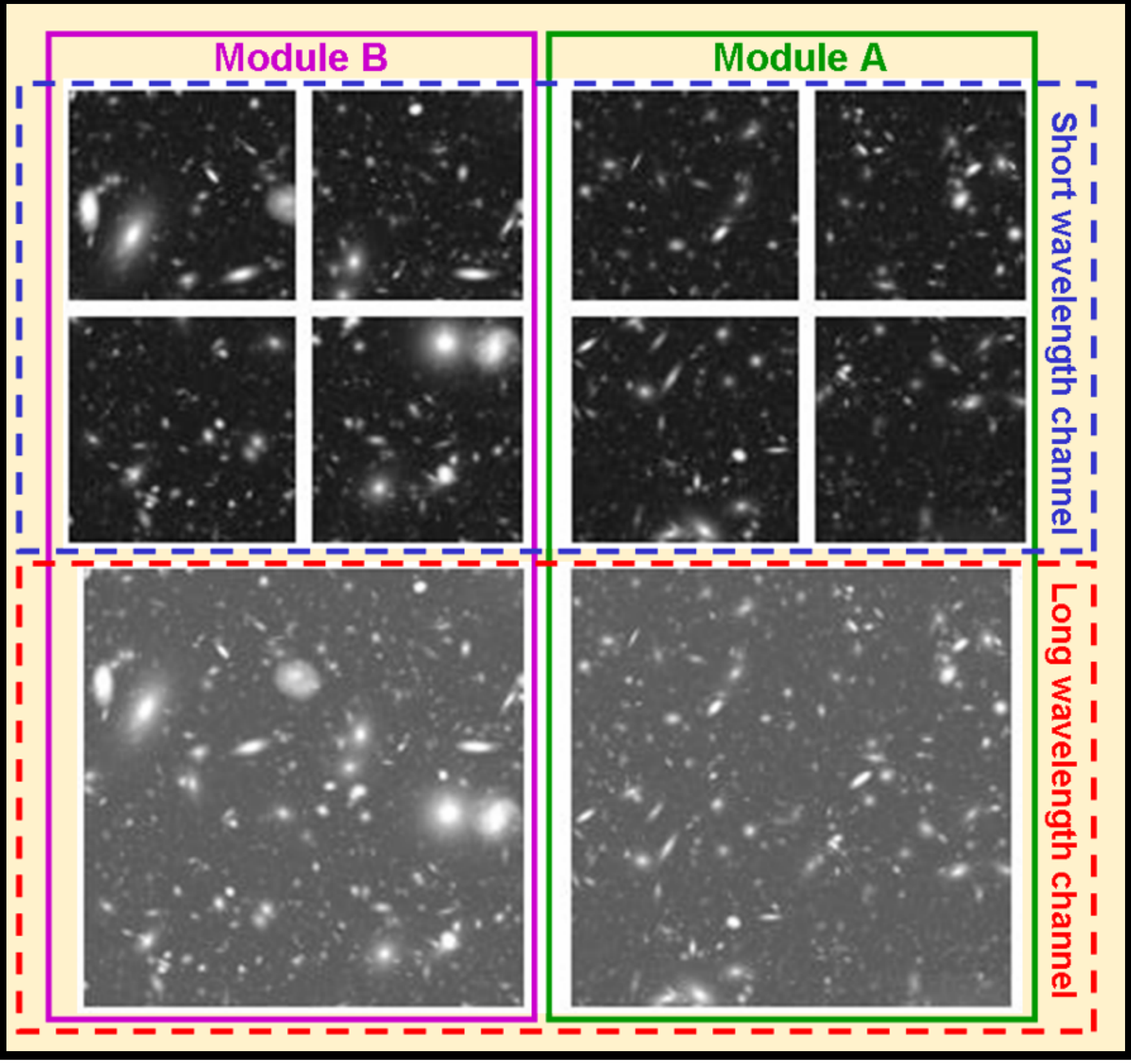

Nebular Emission in High-z Galaxies

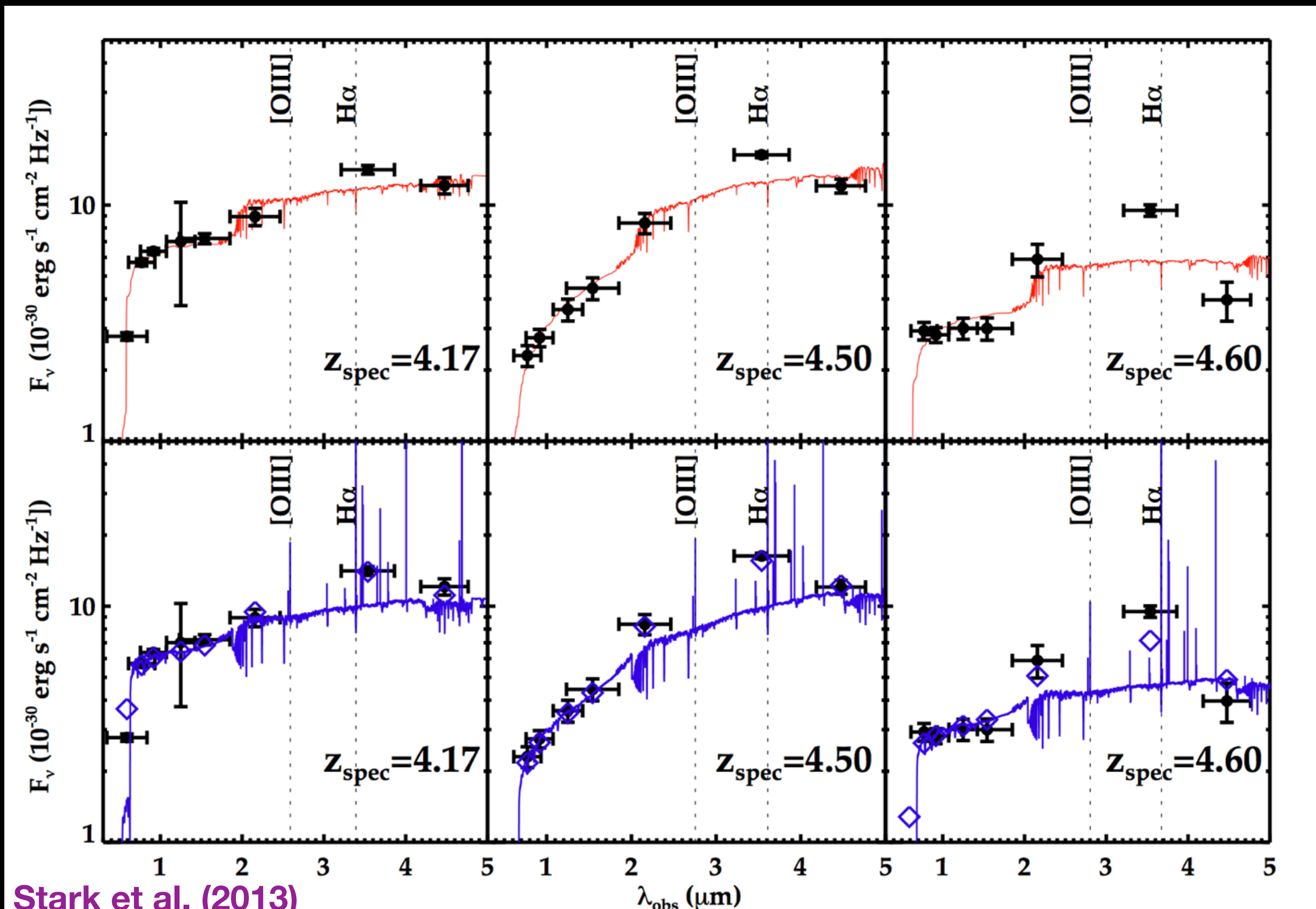

The rest-frame UV photometric data from HST and rest-frame optical data from *Spitzer* enable a fit of stellar population synthesis models to determine stellar masses.

Galaxies in certain redshift windows will have their rest-frame optical photometry affected by nebular line emission.

Nebular continuum emission can also affect rest-frame UV-optical photometry.

See, e.g., Schaerer & de Barros (2009, 2010); Ono et al. (2010); Robertson et al. (2010); Shim et al. (2011); de Barros et al. (2012); Stark et al. (2013), Labbe et al. (2013); de Barros, Schaerer, & Stark (2014); Smit et al. (2014, 2015)

Modeling Nebular Emission

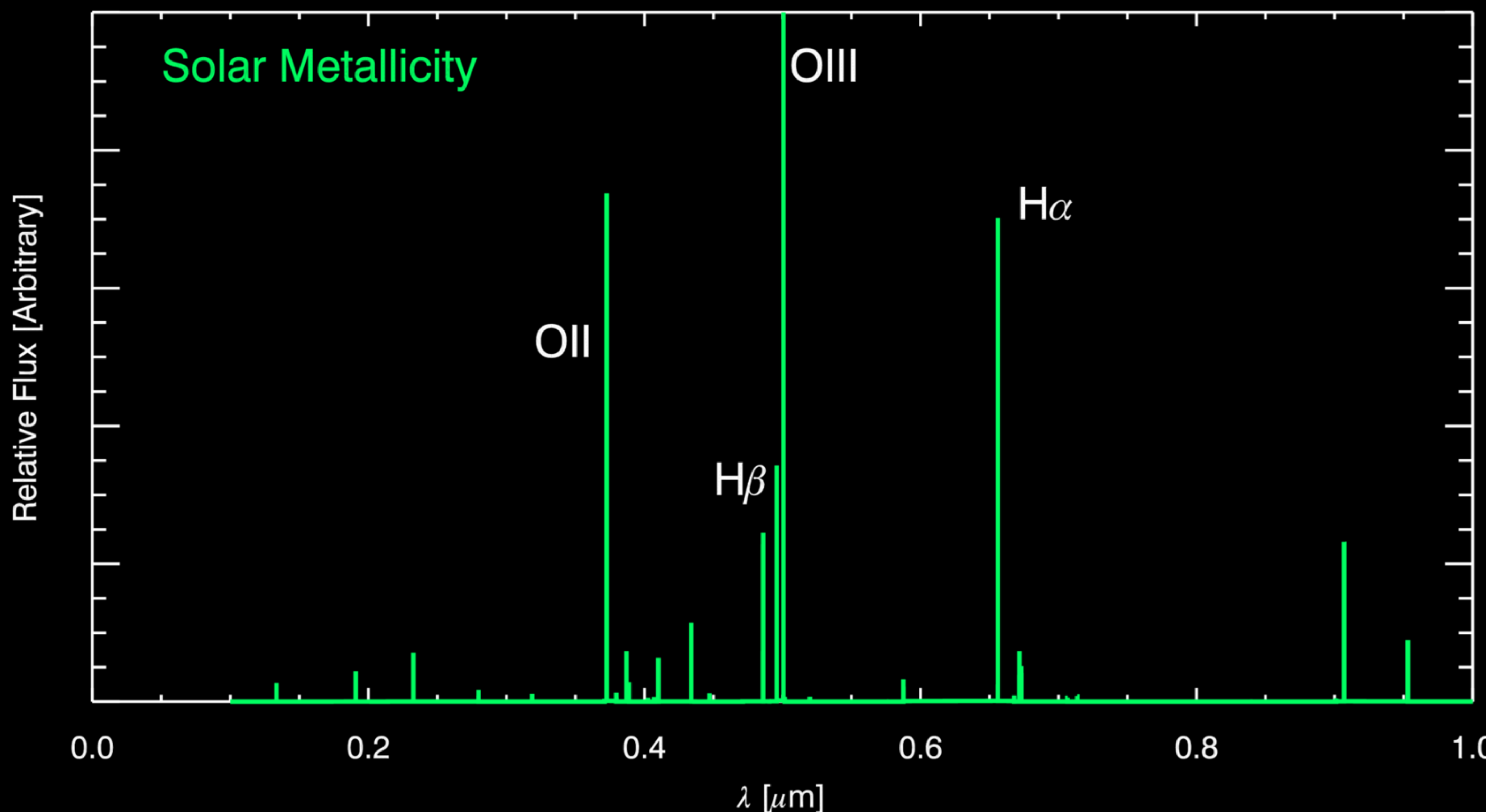

1) Line Emission

$$L(H\beta) = 4.78 \times 10^{-13}(1 - f_{\rm esc})N_{\rm Lyc}[\rm ergs\ s^{-1}]$$

Tie additional lines (He, C, O, N, Mg, Ne, S, Ar) to Hβ luminosity (following Anders & Fritze-v. Alvensleben 2003).

Modeling Nebular Emission

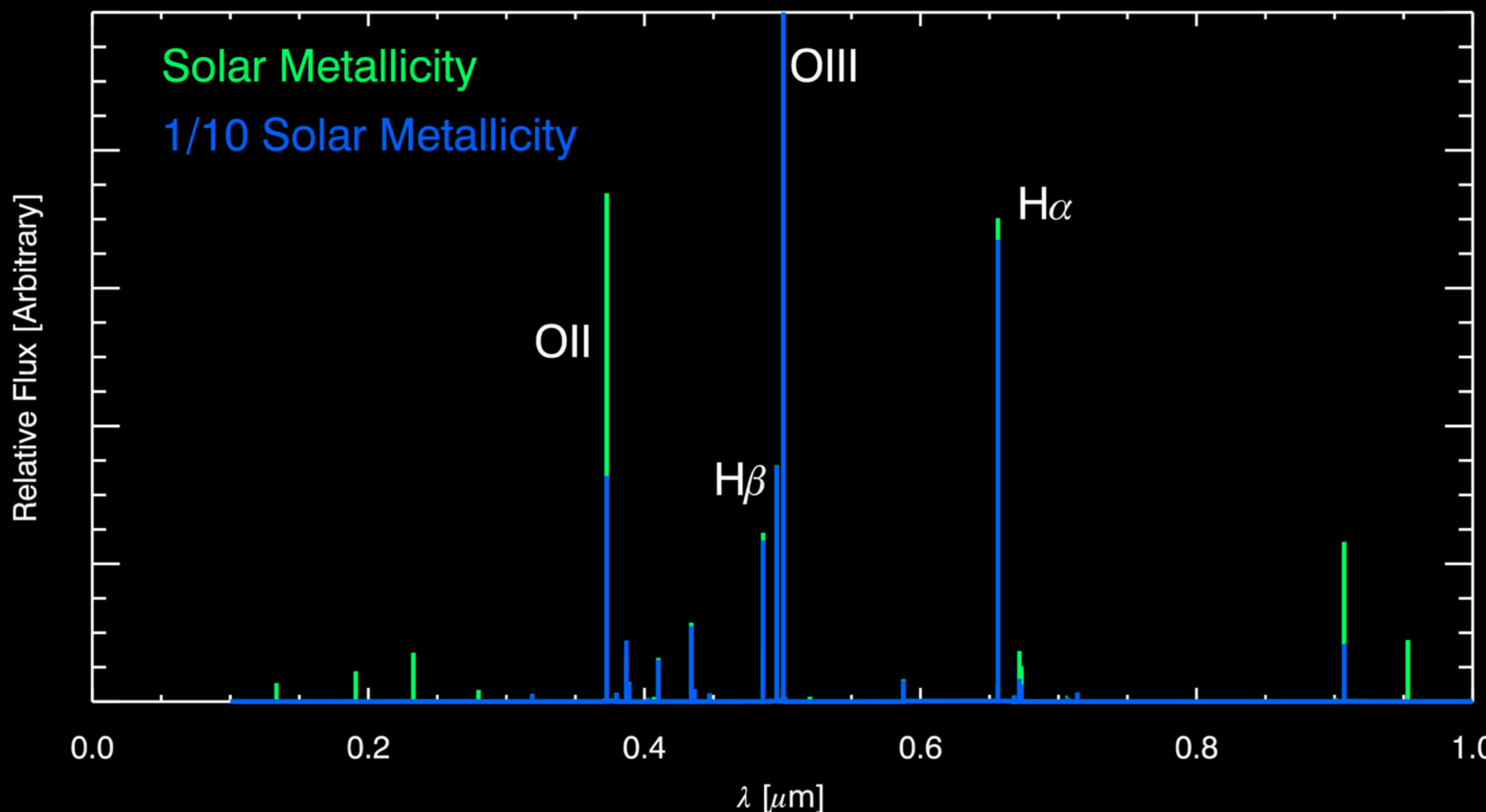

1) Line Emission

$$L(H\beta) = 4.78 \times 10^{-13}(1 - f_{\rm esc})N_{\rm Lyc}[{\rm ergs\ s^{-1}}]$$

Tie additional lines (He, C, O, N, Mg, Ne, S, Ar) to Hβ luminosity (following Anders & Fritze-v. Alvensleben 2003).

Modeling Nebular Emission

1) Line Emission

$$L(H\beta) = 4.78 \times 10^{-13}(1 - f_{\rm esc})N_{\rm Lyc}[\rm ergs\ s^{-1}]$$

Tie additional lines (He, C, O, N, Mg, Ne, S, Ar) to Hβ luminosity (following Anders & Fritze-v. Alvensleben 2003).

2) Continuum Emission

$$L_\nu = \frac{\gamma_\nu}{\alpha_{\rm B}}(1 - f_{\rm esc})N_{\rm Lyc}$$

Nebular continuum emission proportional to Lyman continuum photon production.

Continuum Emission Coefficient

$$\gamma_\nu = \gamma_\nu^{\rm HI} + \gamma_\nu^{2\nu} + \gamma_\nu^{\rm HeI}\frac{n({\rm He}^+)}{n({\rm H}^+)} + \gamma_\nu^{\rm HeII}\frac{n({\rm He}^{++})}{n({\rm H}^+)}$$

Ch. 4 of Osterbrock & Ferland 2006

Nebular Emission Coefficients

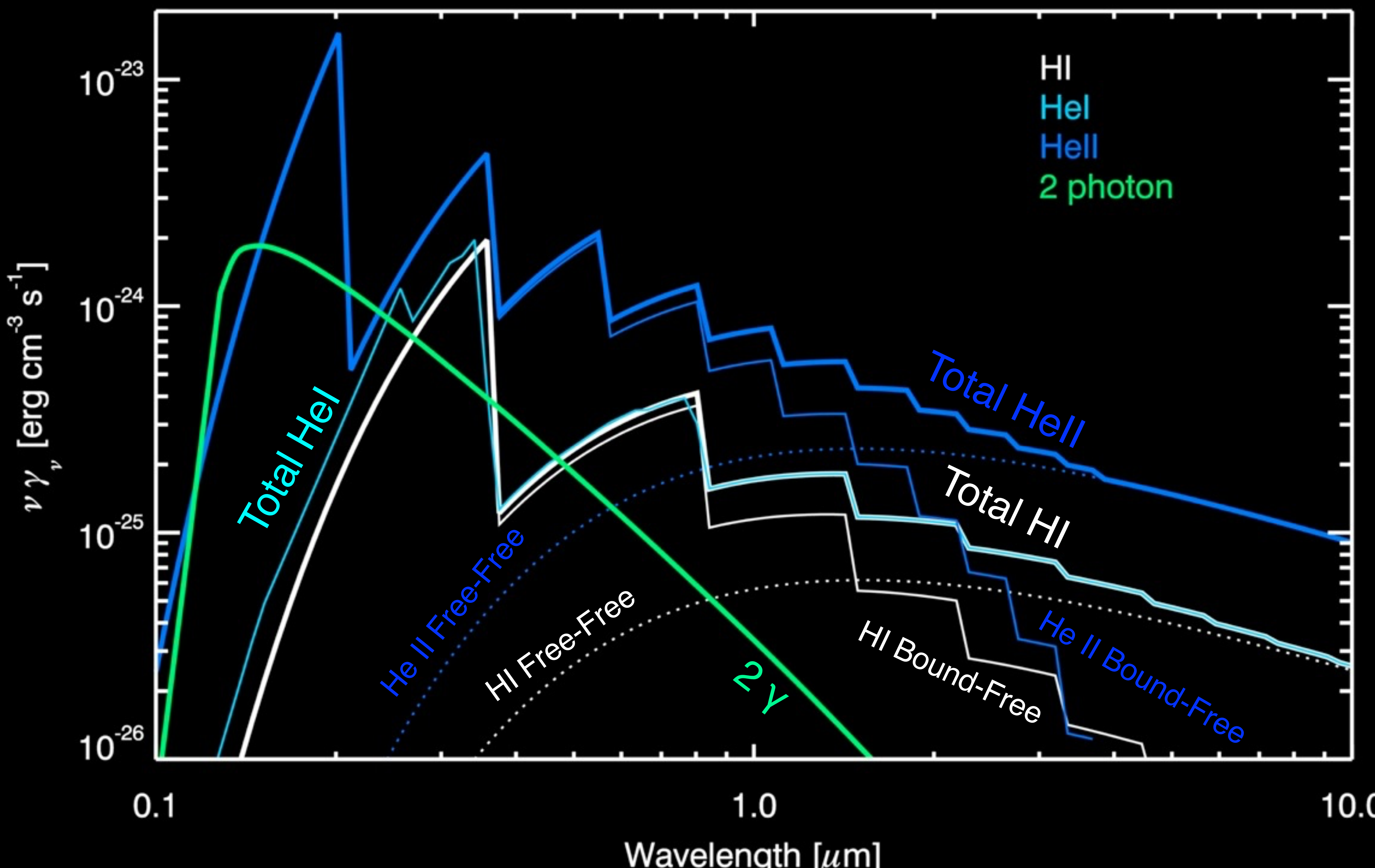

Figure 4.1, Osterbrock & Ferland 2006

$$\gamma_\nu = \gamma_\nu^{\mathrm{HI}} + \gamma_\nu^{2\nu} + \gamma_\nu^{\mathrm{HeI}}\frac{n(\mathrm{He}^+)}{n(\mathrm{H}^+)} + \gamma_\nu^{\mathrm{HeII}}\frac{n(\mathrm{He}^{++})}{n(\mathrm{H}^+)}$$

Standard SED Modeling of High-z Galaxies

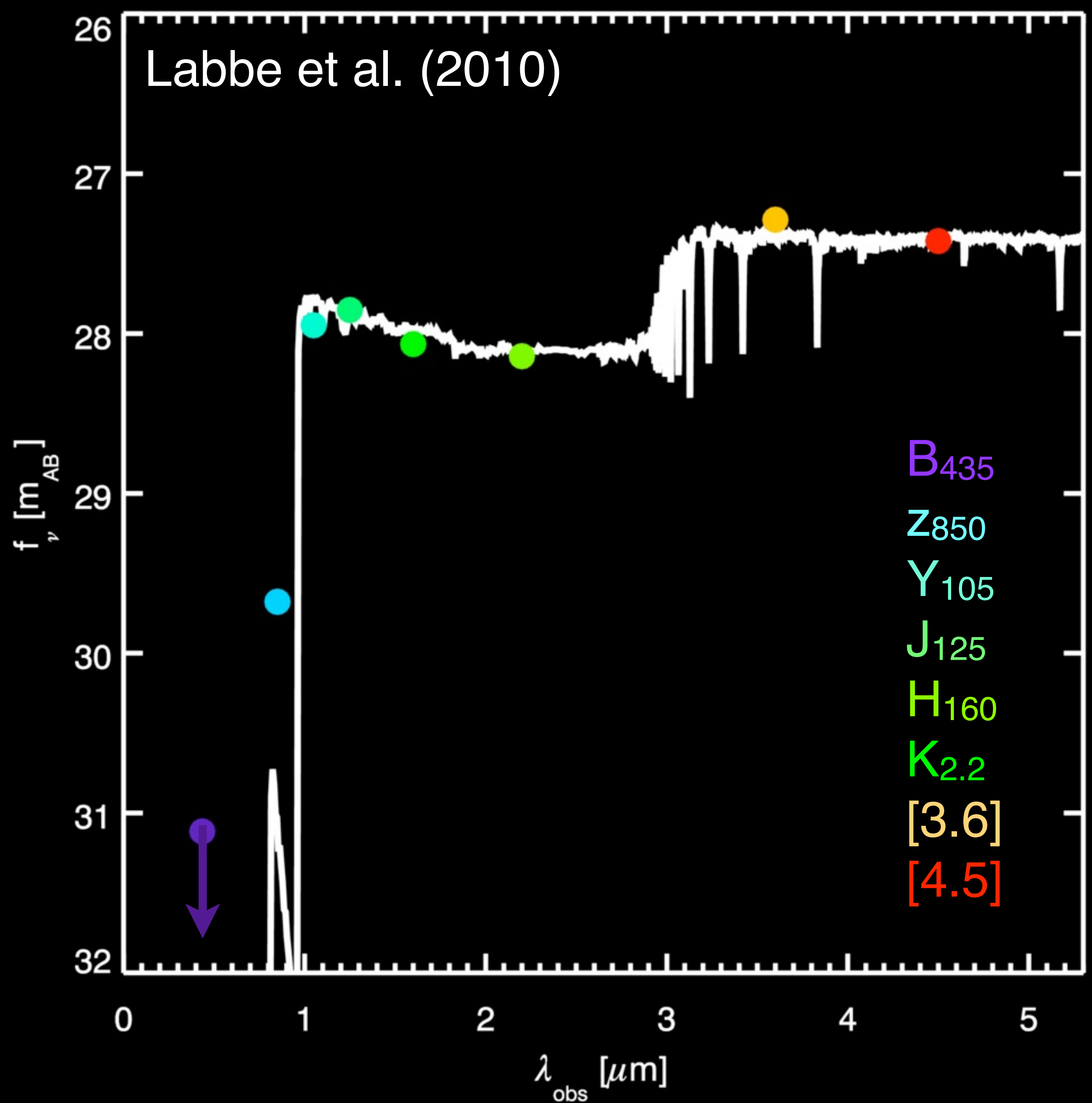

The rest-frame UV photometric data from HST and rest-frame optical data from *Spitzer* enable a fit of stellar population synthesis models.

Best-fit Bruzual & Charlot 2003 model for stacked data:

Age = 4×10^8 yrs
SFR = 2 M_{sun} / yr
$M_\star = 1.25 \times 10^9\ M_{sun}$

SED Modeling of High-z Galaxies Including Nebular Emission

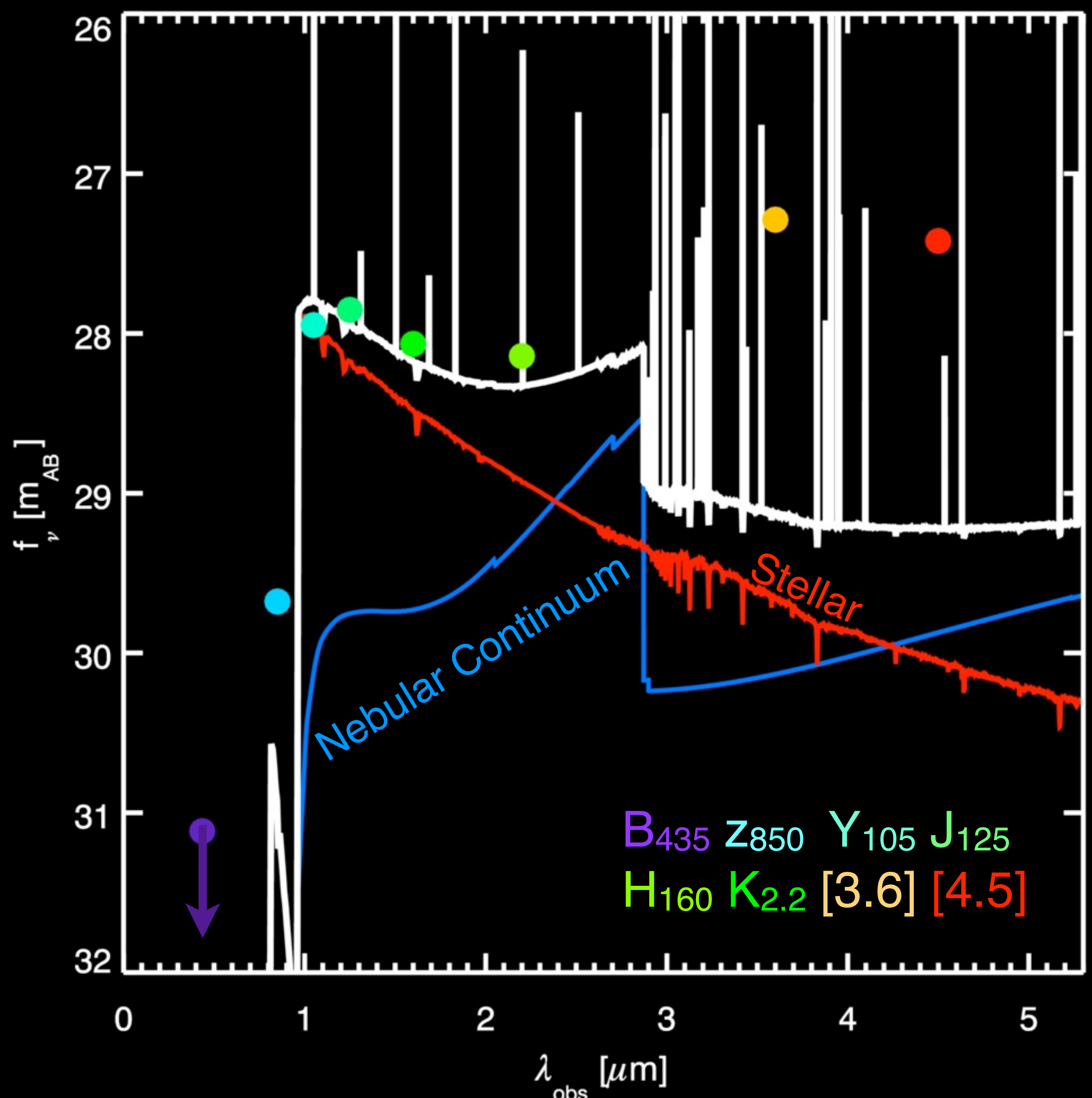

Nebular emission models can fit the photometry equally well, or better than stellar only models. Even seemingly ridiculous ones.

Best-fit Bruzual & Charlot 2003 model + neb. emission (f_{esc}=0) for stacked data:

Age = 1.45 x 10^6 yrs
SFR = 36 M_{sun} / yr
$M_\star$ = 5.25 x 10^7 M_{sun}

Constraints on the nebular emission are going to be necessary to constrain tightly stellar mass at high-z.

Connecting Line Diagnostics in High Redshift Galaxies Across Wavelengths

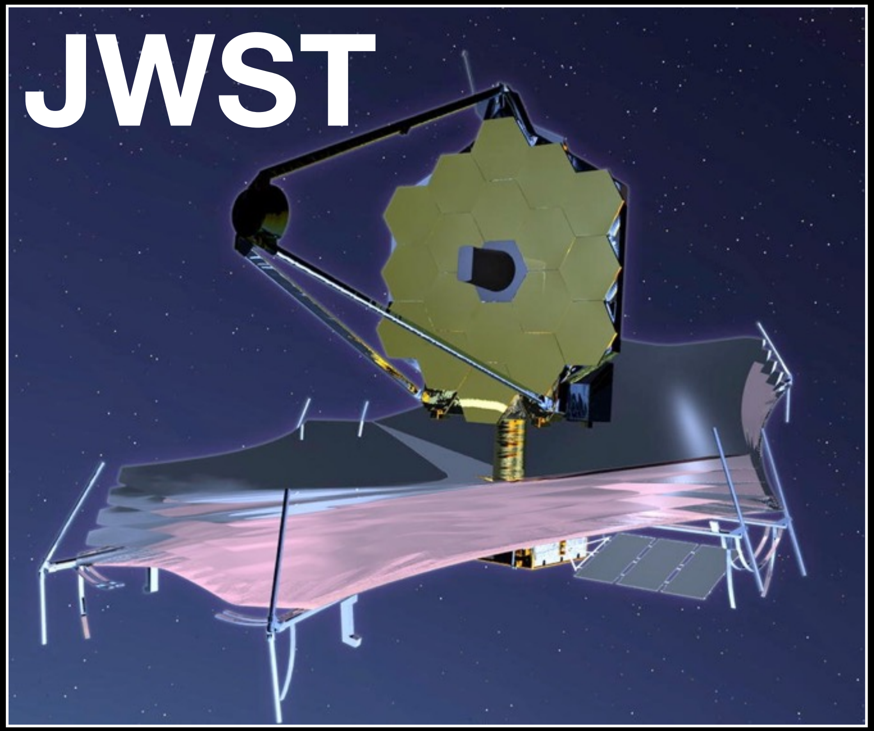

What can we learn by combining observations from these two facilities?

High-z Star-Forming Galaxies are Strong UV-Optical Line Emitters

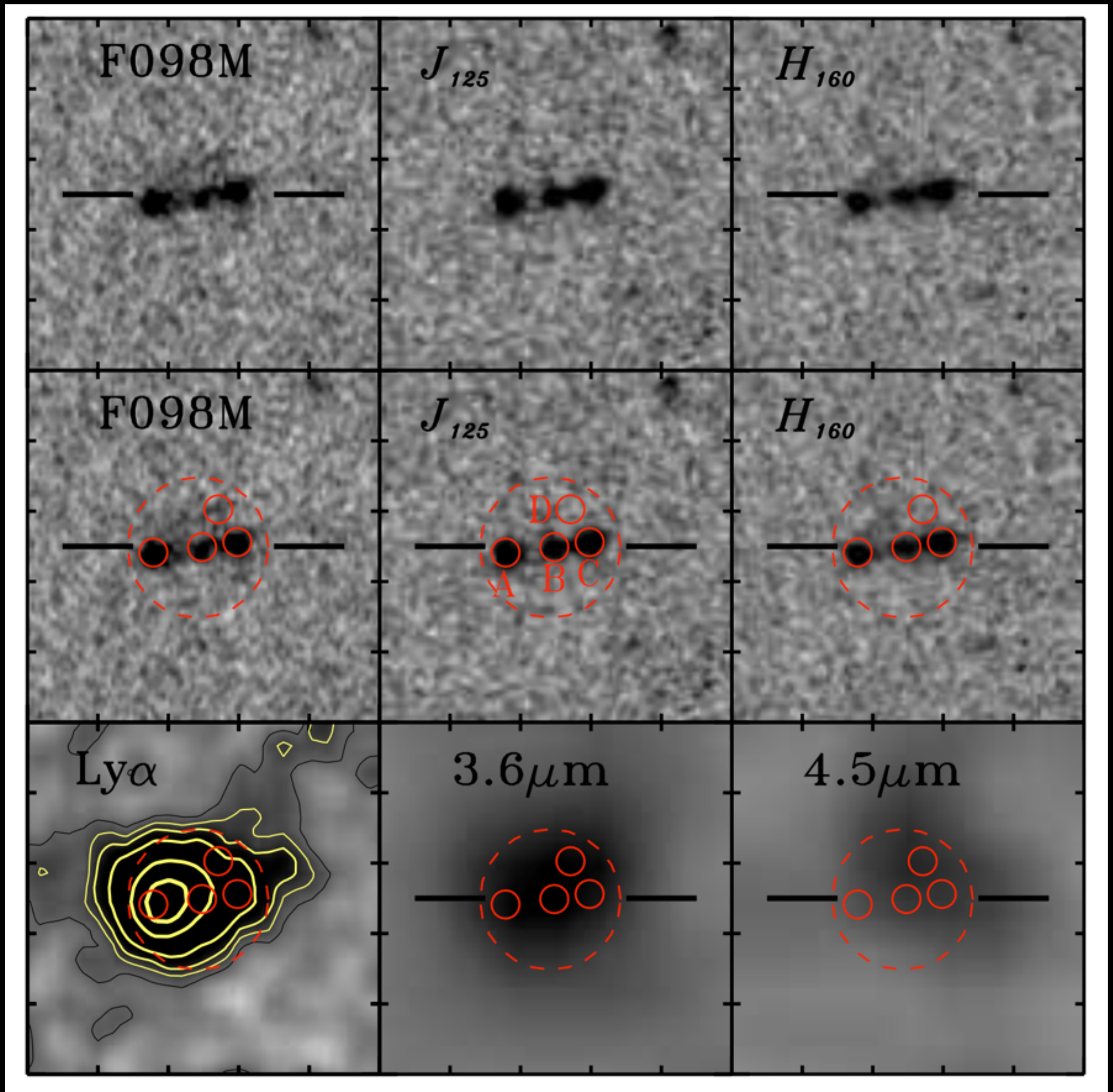

HST + Spitzer + NBLya

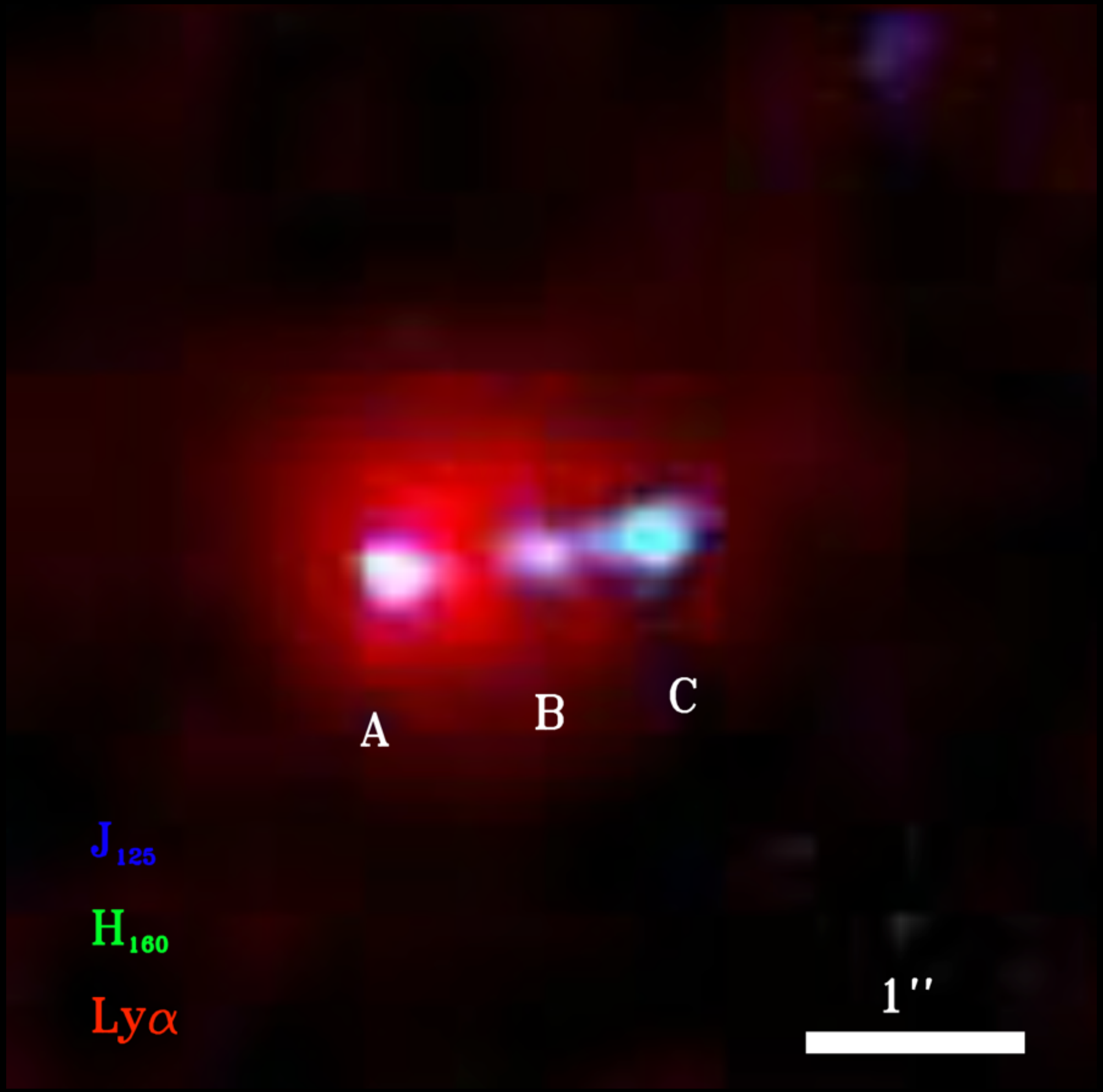

Ouchi et al. (2013)

Himiko Lya Emitter @ z~6.6

Far IR Emission(?) from High-z Galaxies

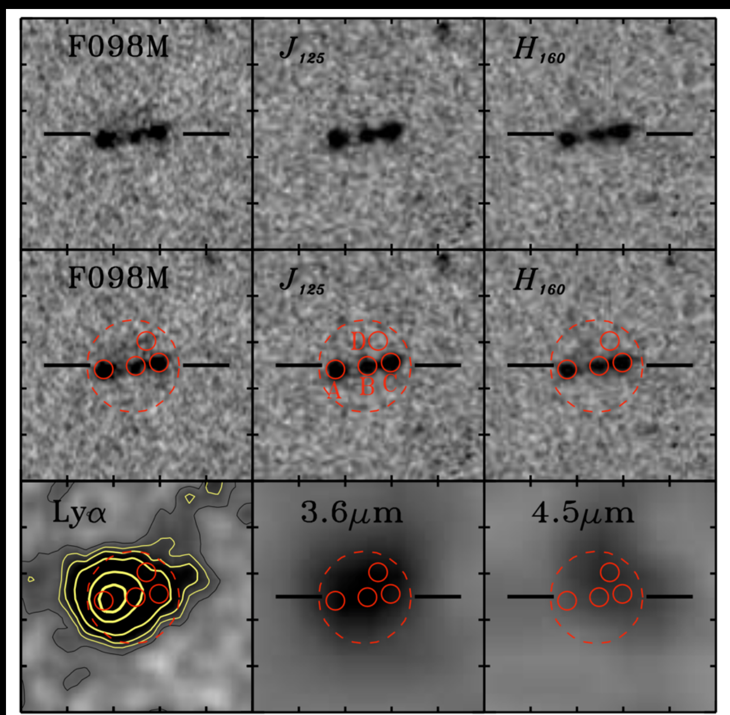

HST + Spitzer + NBLya

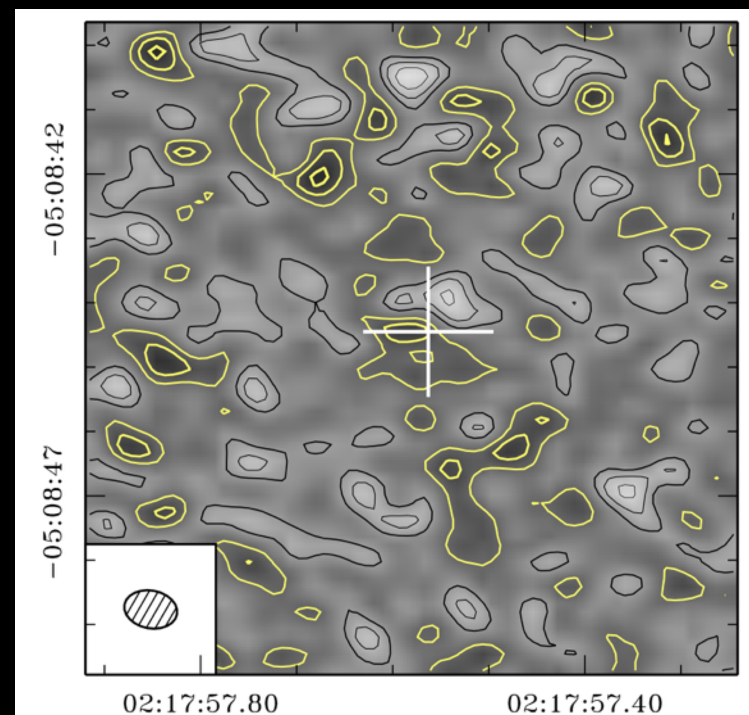

ALMA Continuum Map

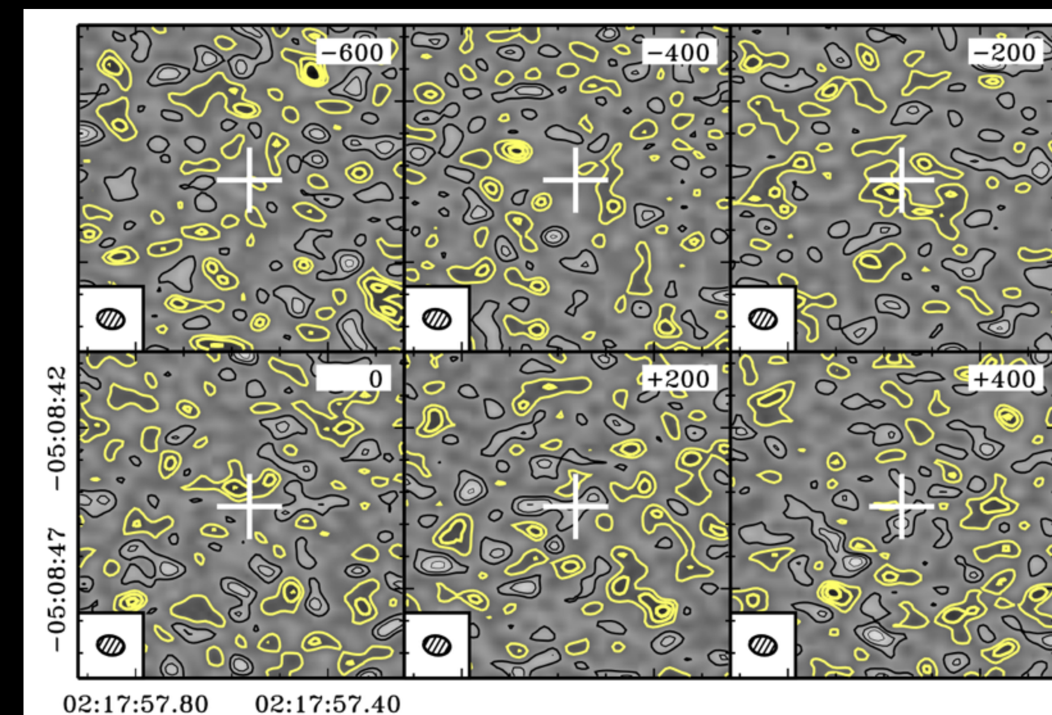

ALMA [CII] Velocity Channel Maps

Himiko Lya Emitter @ z~6.6

Ouchi et al. (2013)

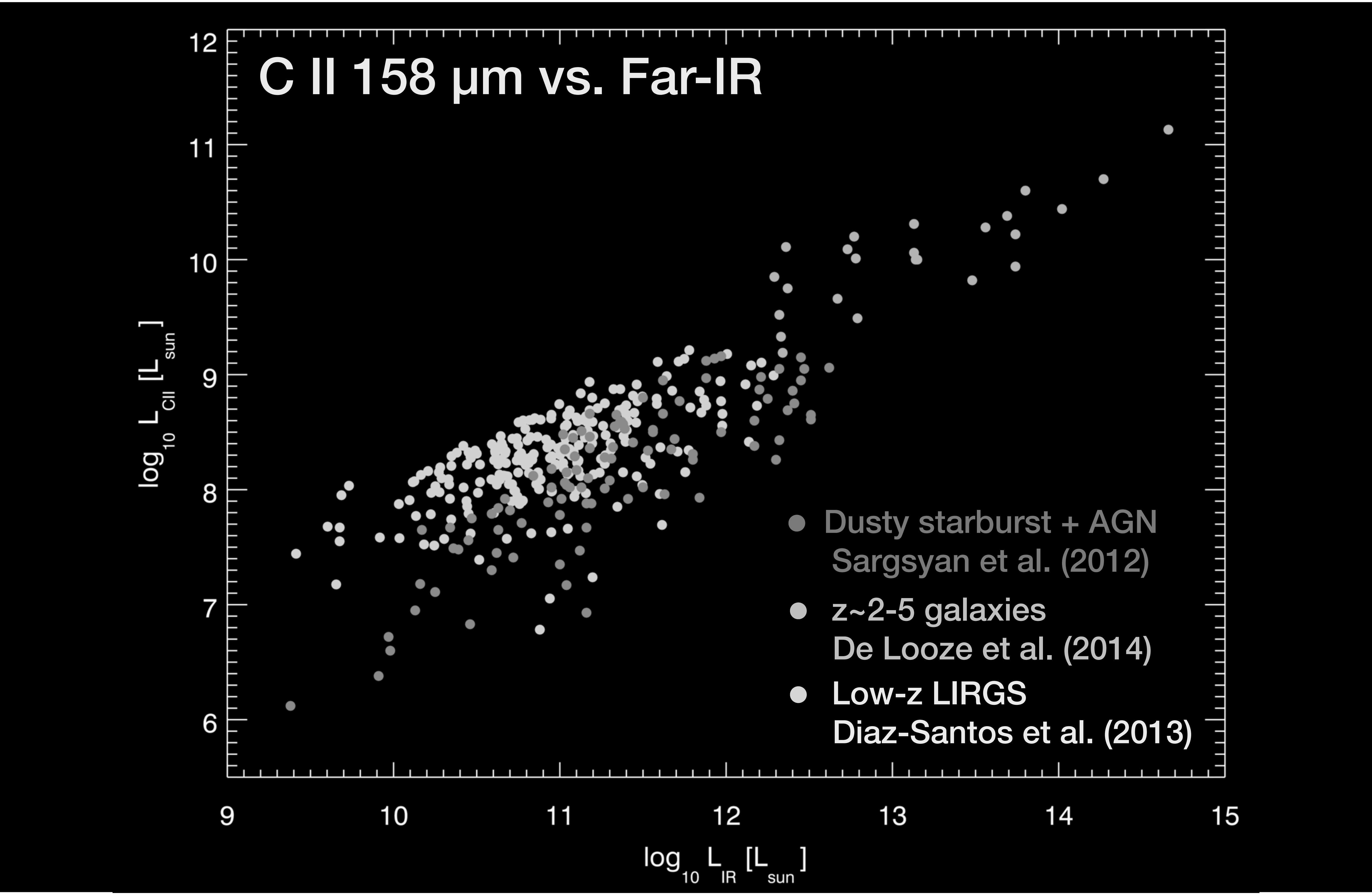
C II 158 μm vs. Far-IR
12
11
10
9
8
7
6
log10 LCII [Lsun]
9
10
11
12
13
14
15
log10 LIR [Lsun]
Dusty starburst + AGN
Sargsyan et al. (2012)
z~2-5 galaxies
De Looze et al. (2014)
Low-z LIRGS
Diaz-Santos et al. (2013)

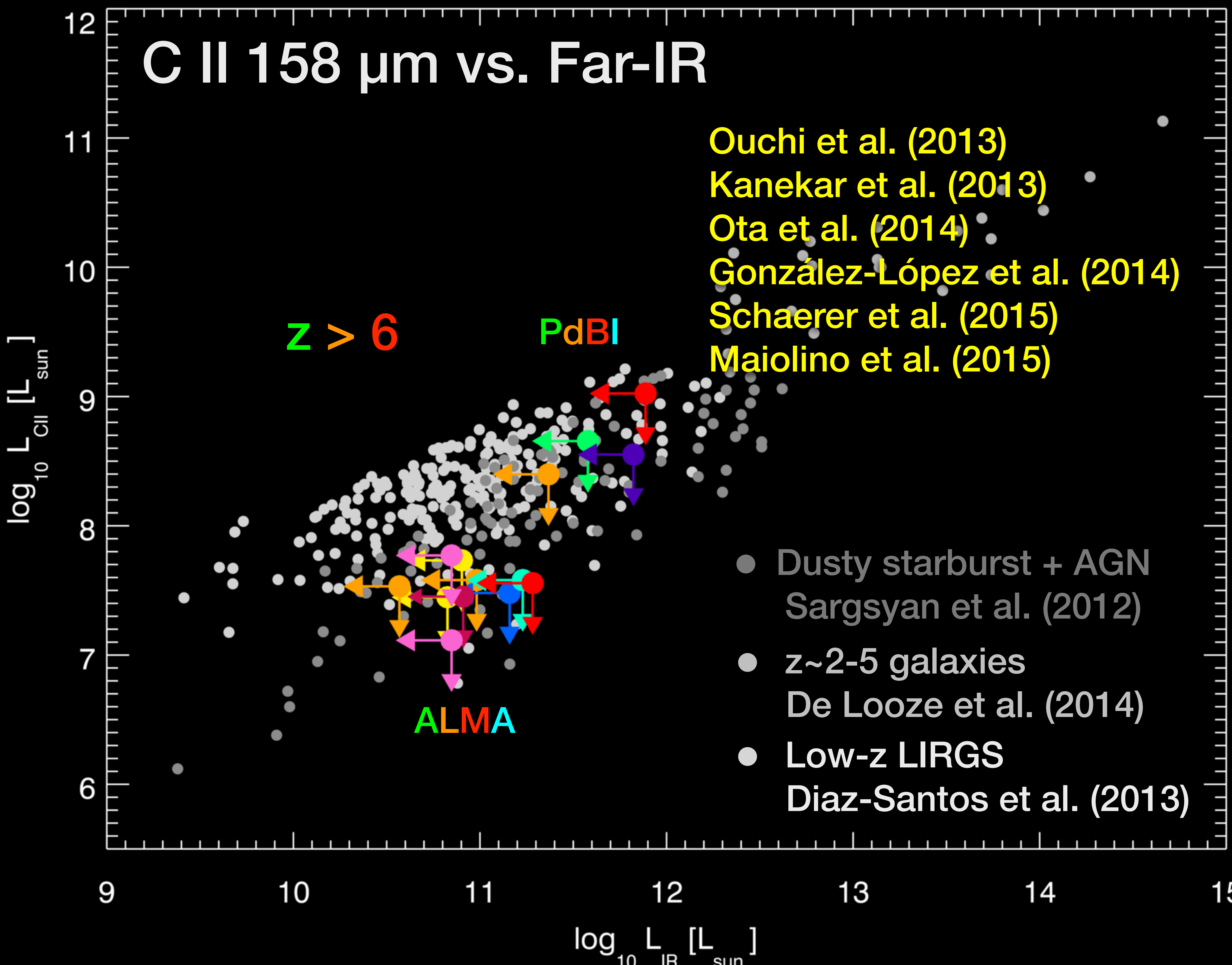
C II 158 μm vs. Far-IR
Ouchi et al. (2013)
Kanekar et al. (2013)
Ota et al. (2014)
González-López et al. (2014)
Schaerer et al. (2015)
Maiolino et al. (2015)
z > 6
PdBI
ALMA
Dusty starburst + AGN
Sargsyan et al. (2012)
z~2-5 galaxies
De Looze et al. (2014)
Low-z LIRGS
Diaz-Santos et al. (2013)
$\log_{10} L_{CII}$ [L_{sun}]
$\log_{10} L_{IR}$ [L_{sun}]
12
11
10
9
8
7
6
9
10
11
12
13
14
15

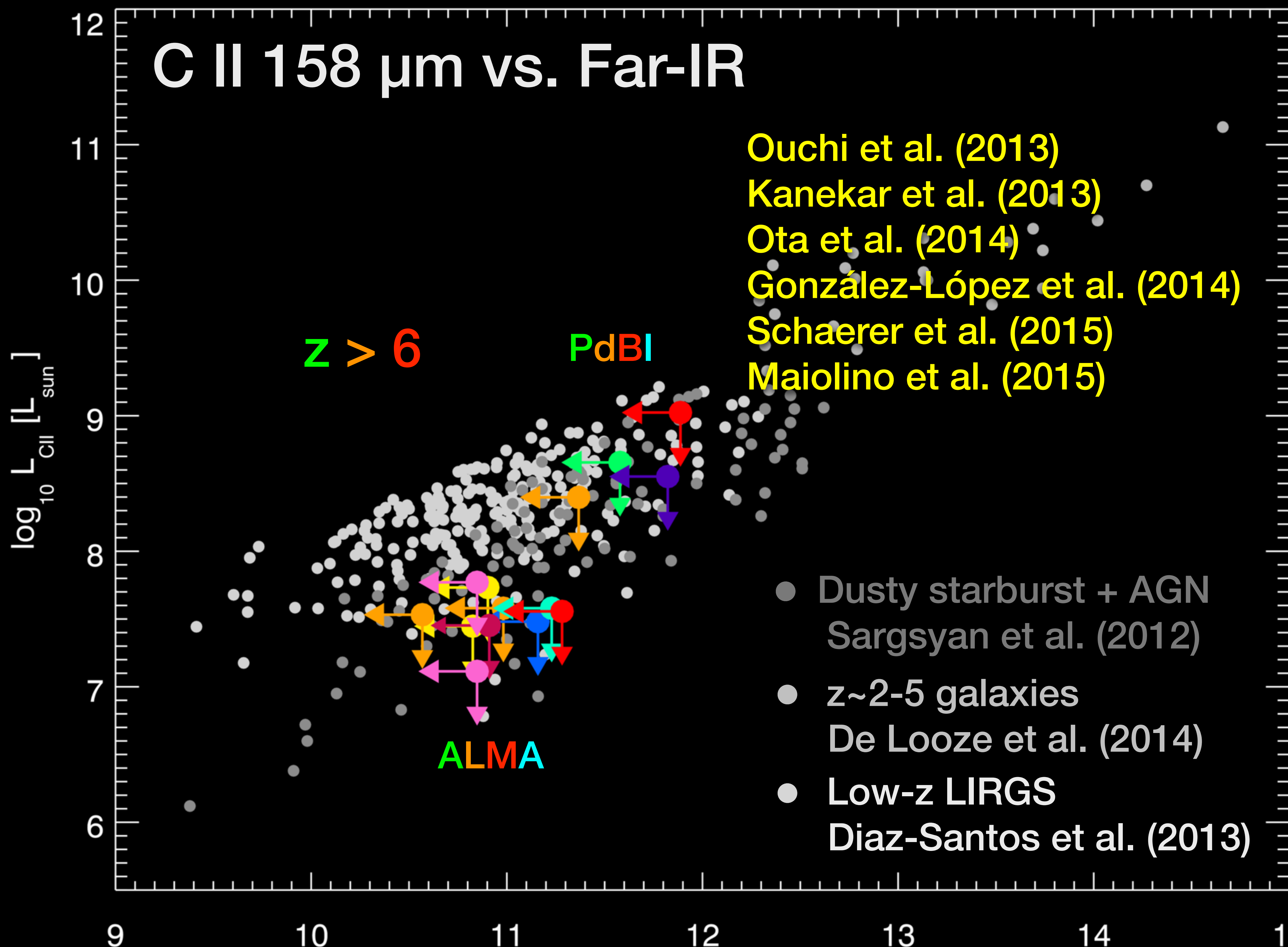

See also Venemans et al. (2012), Carilli et al. (2013), Wagg et al. (2012), Carniani et al. (2013), Williams et al. (2014), Riechers et al. (2014), Rawle et al. (2014), De Brueck et al. (2014), Ferkinhoff et al. (2014), Hyunh et al. (2014), Swinbank et al. (2012, 2014), Wang et al. (2013), Willott et al. (2015)

CII 158 μm vs. Star Formation Rate

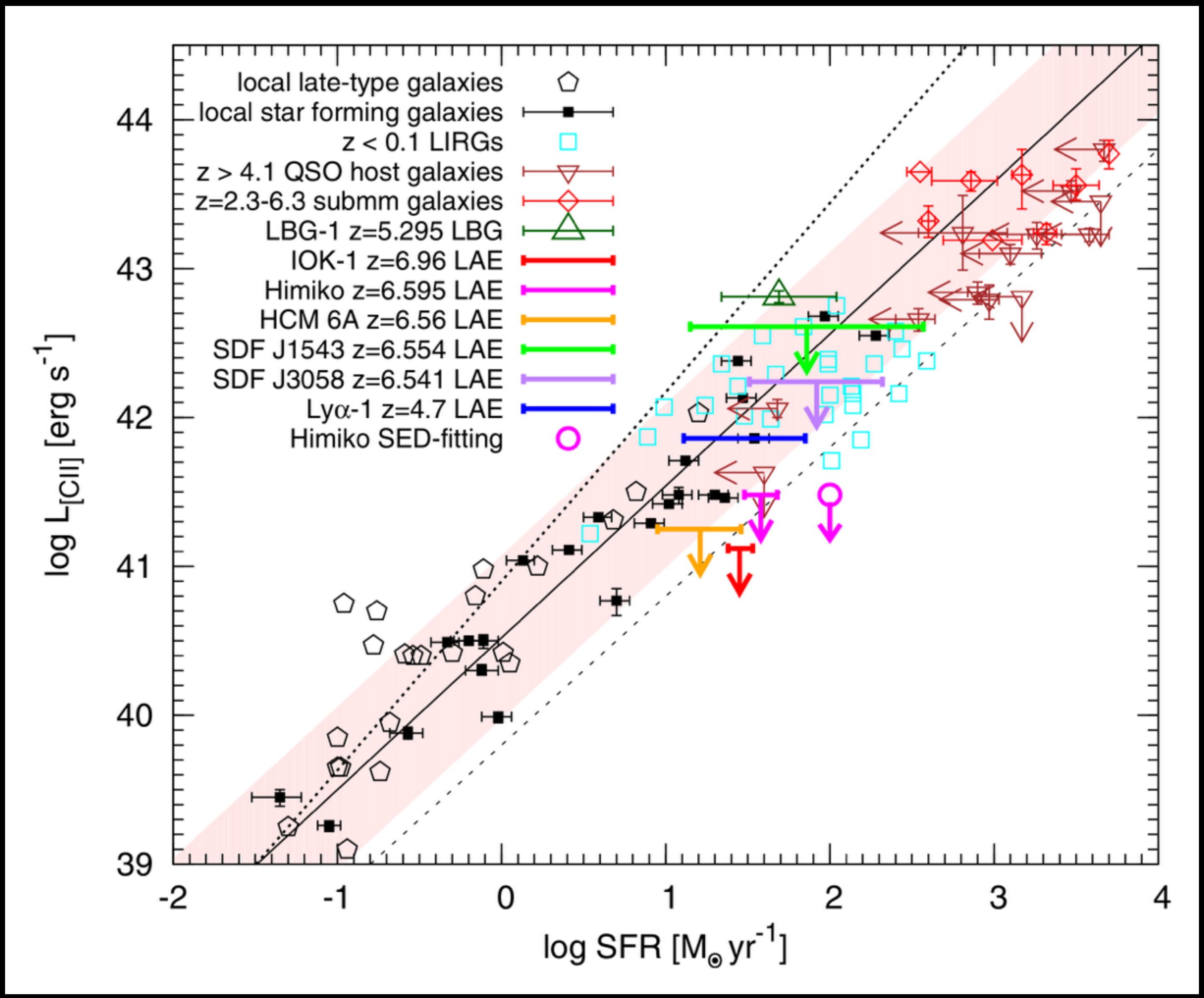

Ota et al. (2014)

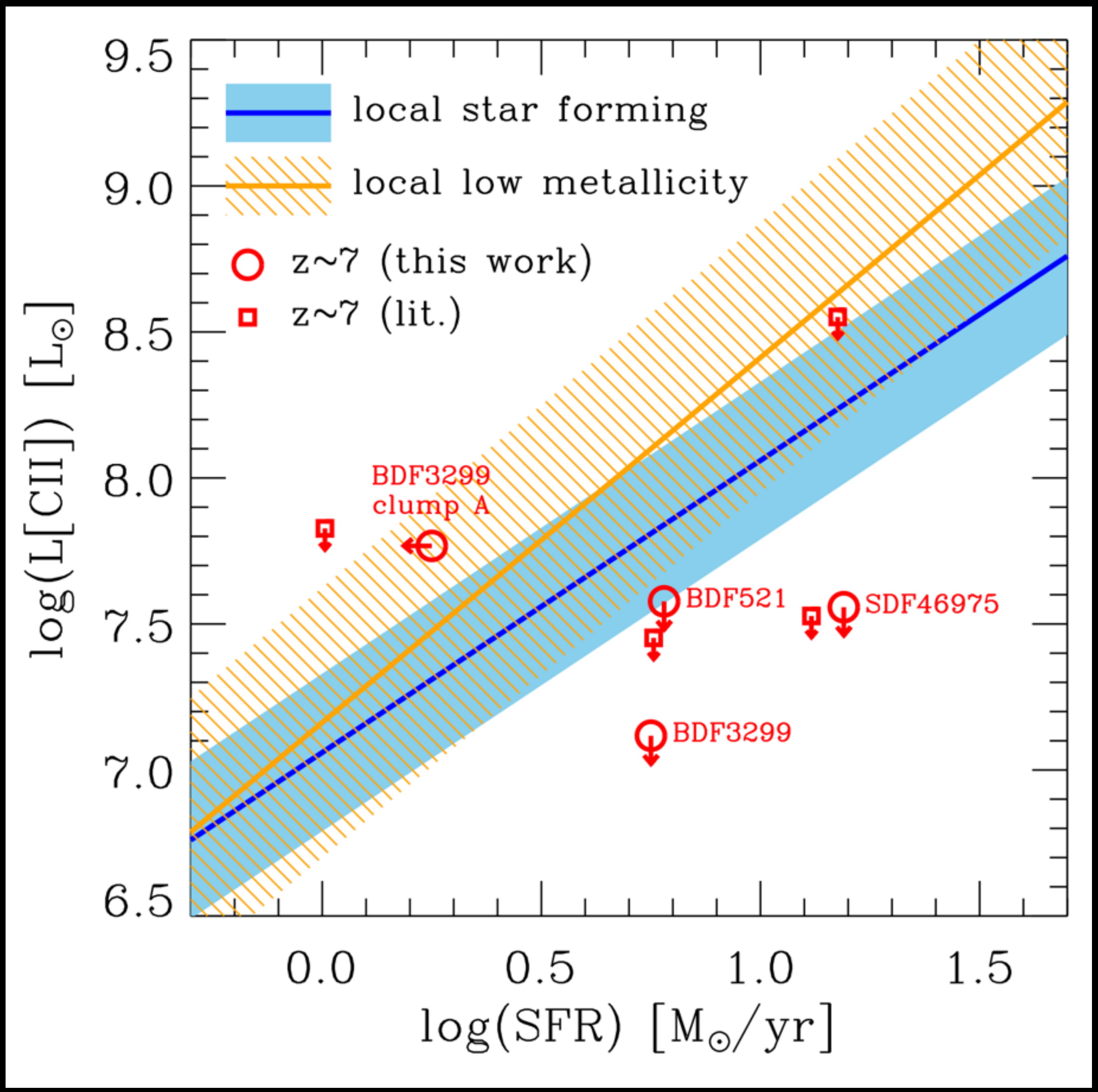

Maiolino et al. (2015)

Collisional Excitation of CII 158 μm

Goldsmith et al. (2012), ApJS, 203, 13

Two-level model of collisional excitation of C^+ with H, H_2, e^-.

Over a wide range of C^+ columns, emission increases with optical depth even when the line is optically thick.

Emission increases with kinetic temperature, and decreases with T of background radiation field (e.g., CMB).

Emission increases with ratio C_{ul}/A_{ul}, the collisional de-excitation vs. spontaneous emission rates.

Zero-excitation optical depth ~ C^+ column density:

$$\tau_0 = 7.49 \times 10^{-18}\ N(\mathrm{C}^+)/\delta v\ (\mathrm{km\ s}^{-1})$$

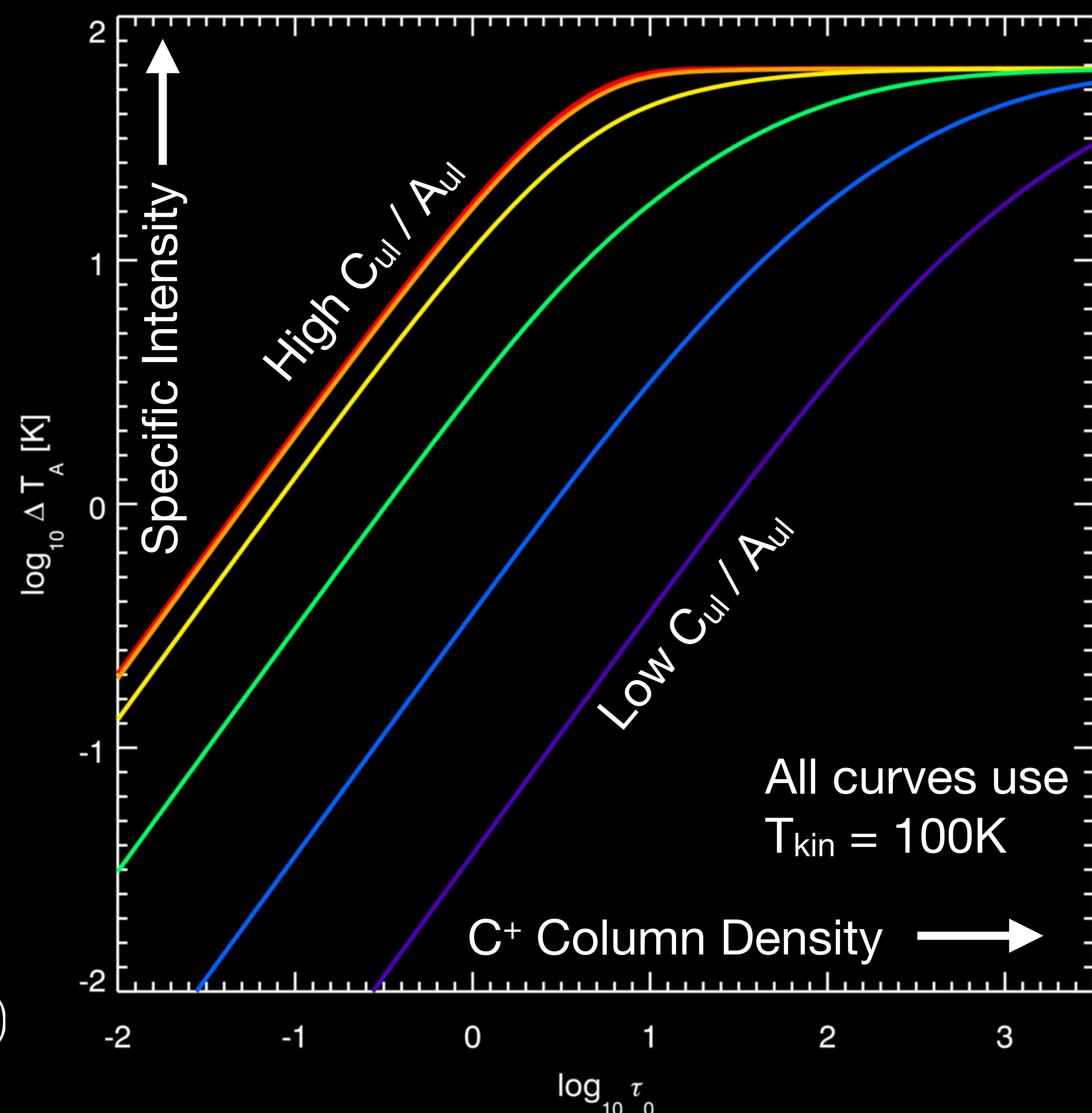

https://github.com/brantr/c-plus

Photodissociation Region Diagnostics

Kaufman et al. (1999), ApJ, 527, 795

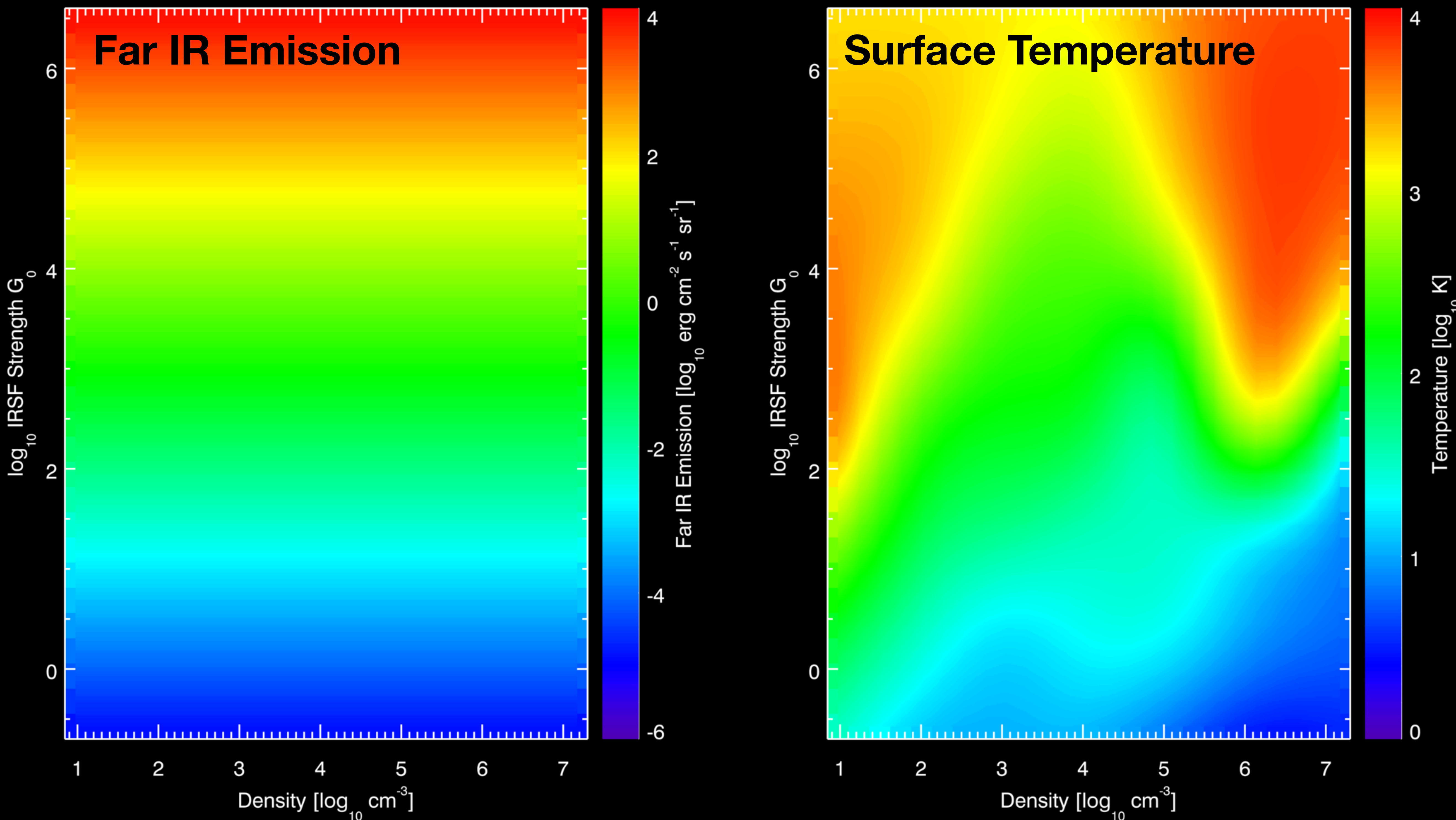

Photodissociation Region Diagnostics

Kaufman et al. (1999), ApJ, 527, 795

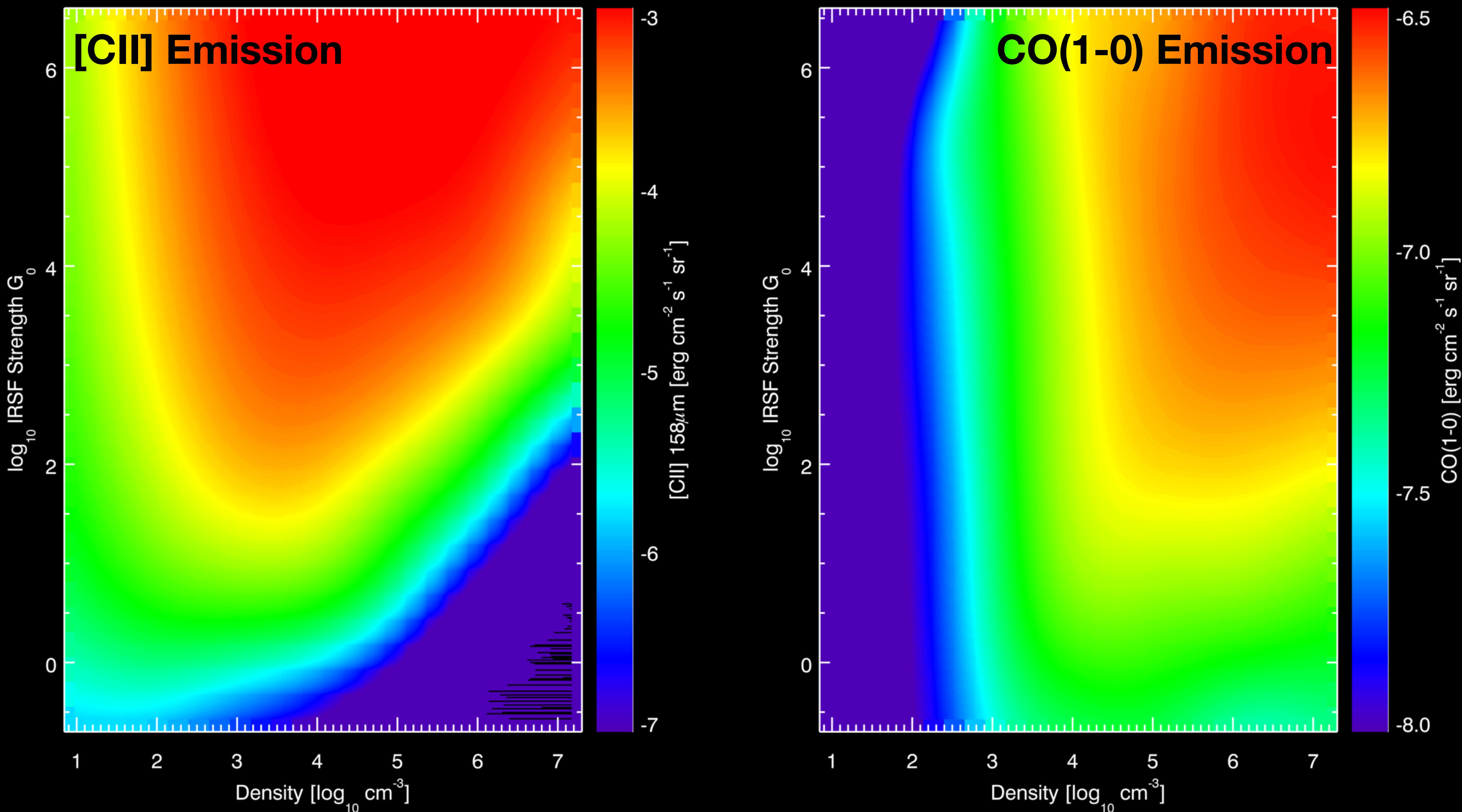

Photodissociation Region Diagnostics

Kaufman et al. (1999), ApJ, 527, 795

n = density
G_0 = ISRF

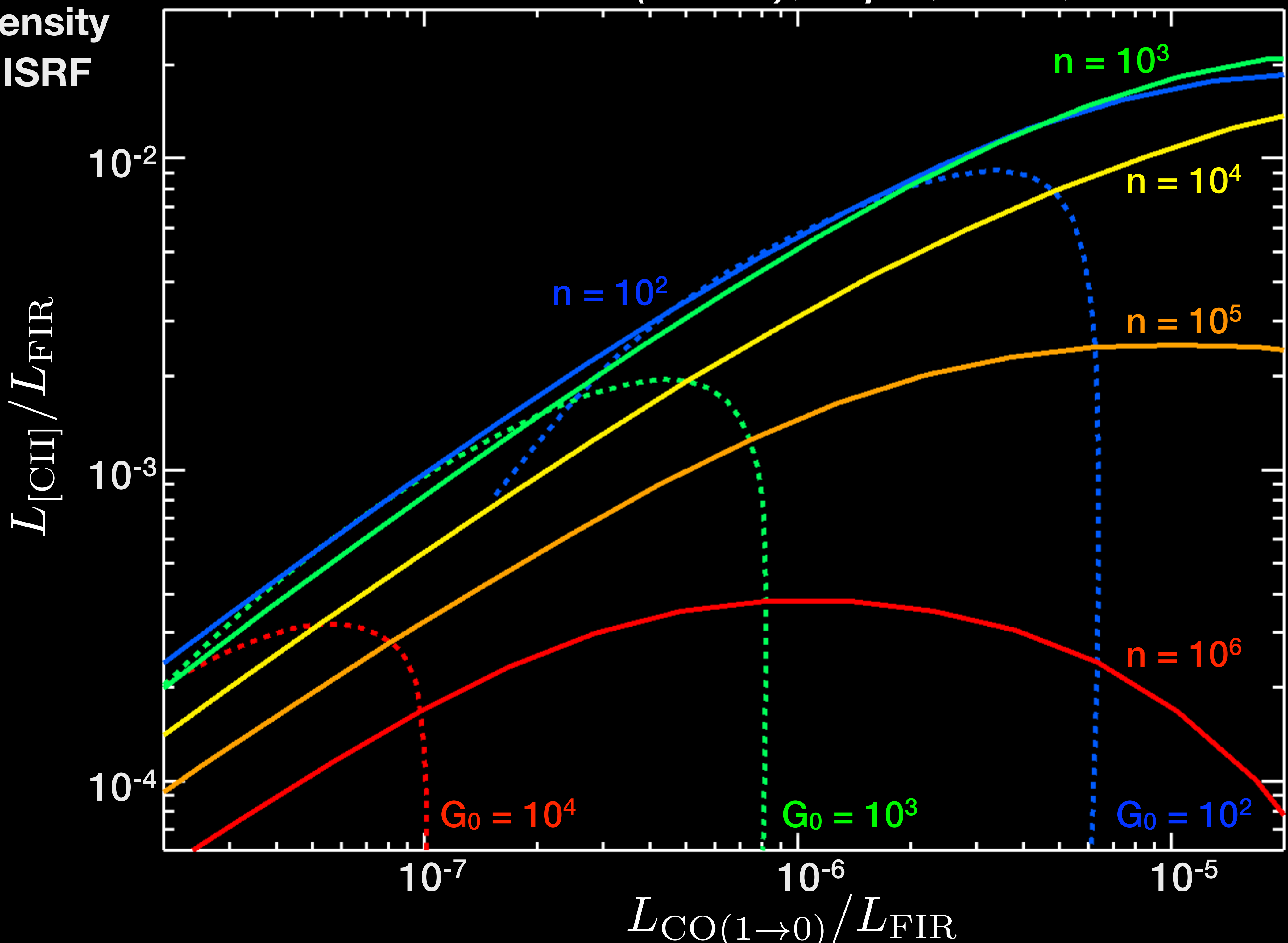

Photodissociation Region Diagnostics

Kaufman et al. (1999), ApJ, 527, 795

n = density
G_0 = ISRF

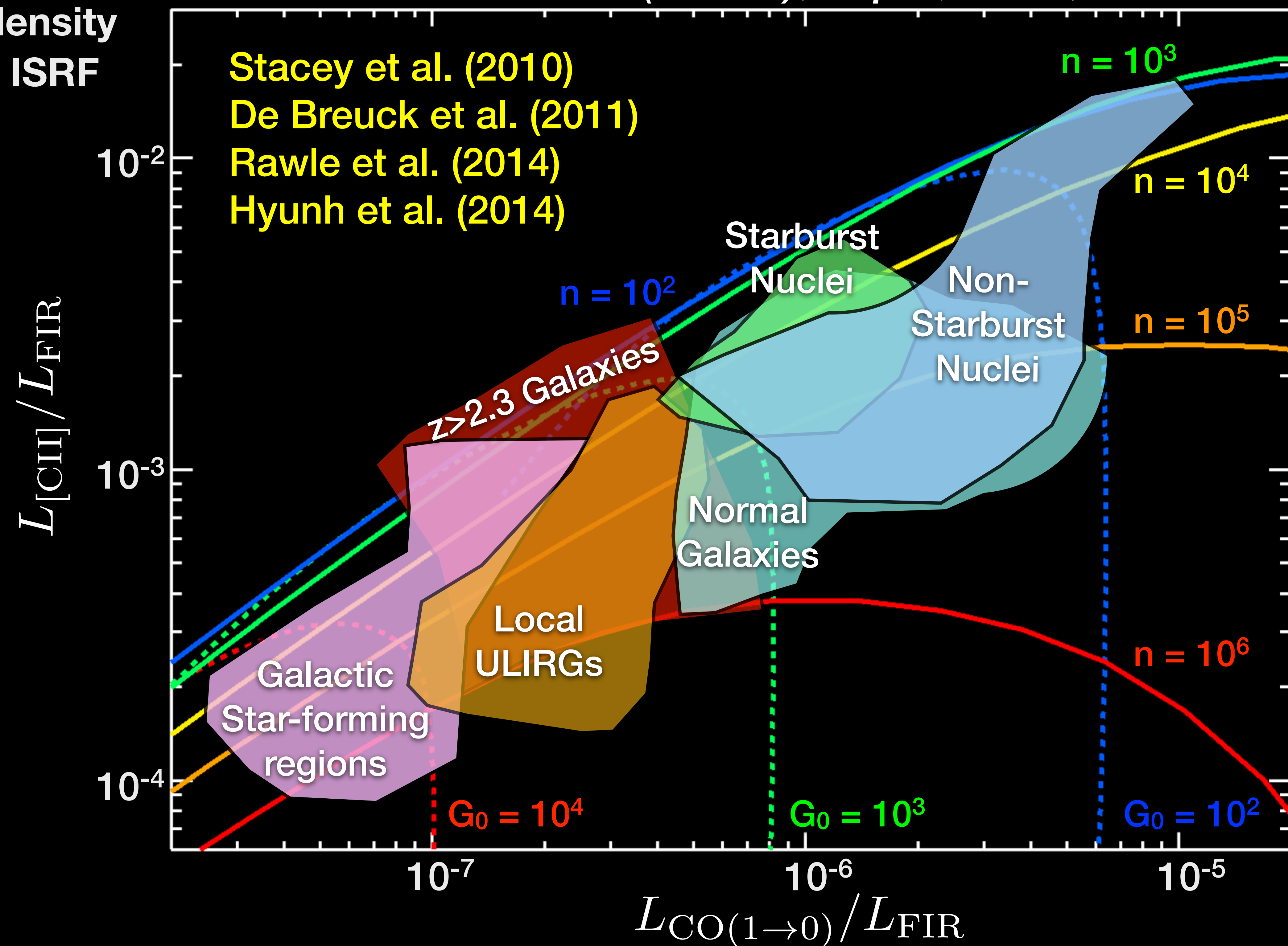

LOTS of Information in the Rest-Frame Submillimeter!

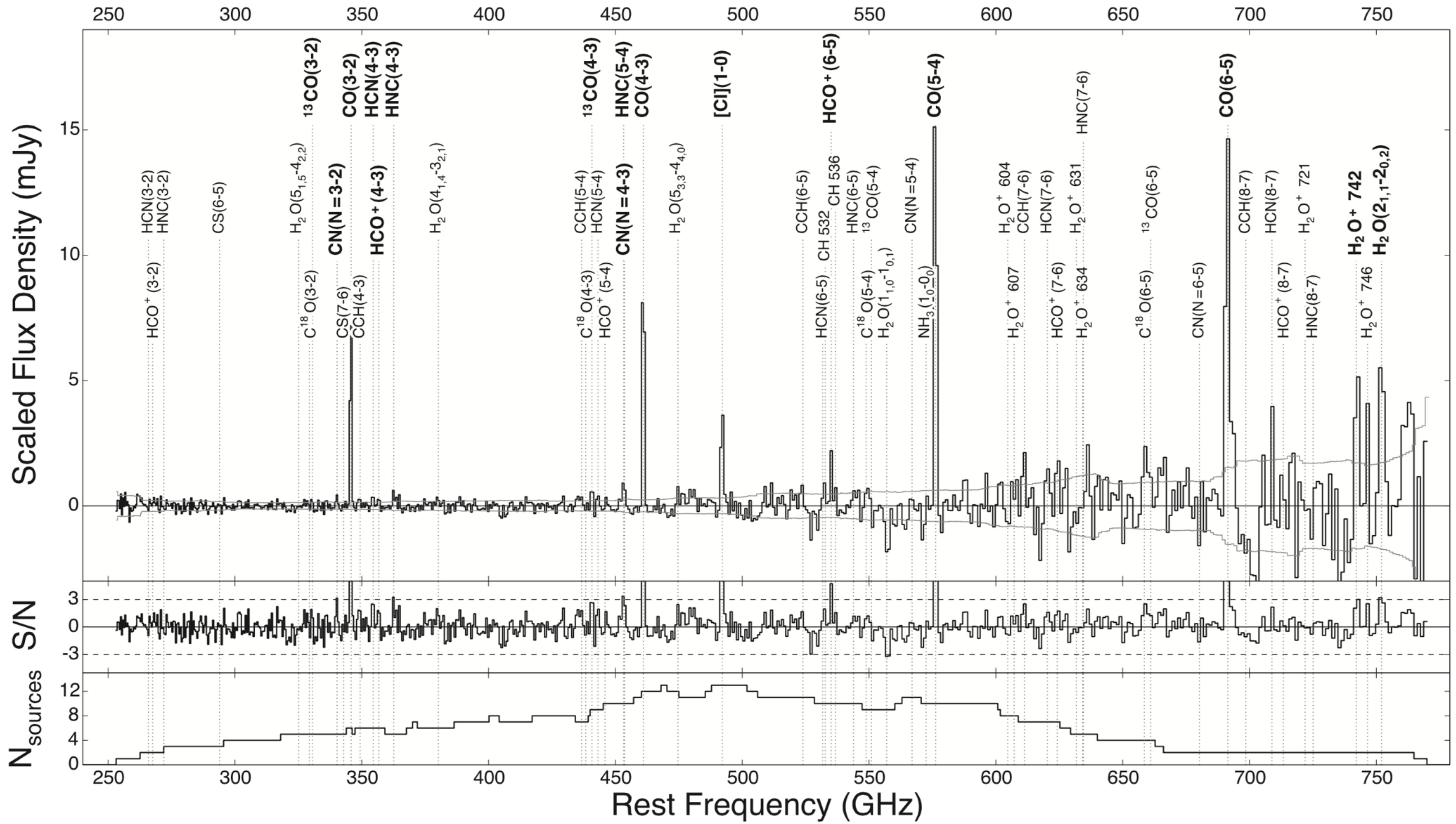

Spilker et al. (2014)

SUMMARY : Early Galaxy Formation and Evolution Through the Eyes of New Facilities

UDF12 Team / NASA / ESA / STScI

- In the last 5 years, a new population of high-redshift galaxies have been discovered out to z~10, informing us about the role of galaxies in reionization.
- Current uncertainties about the properties of high-redshift galaxies include the production rate of ionizing photons and the fraction that escape to ionize the IGM.
- Strong line emission in the UV-optical is inferred for many high-redshift galaxies, will be confirmed with JWST.
- The combined power of ALMA and JWST will teach us a lot about the ISM conditions of high-redshift galaxies and the nature of their stellar populations.